Weather and Climate Extremes 44 (2024) 100669

Contents lists available at ScienceDirect

Weather and Climate Extremes

journal homepage: www.elsevier.com/locate/wace

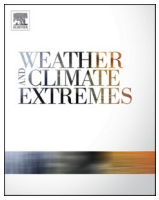

Investigating the spatial and temporal characteristics of compound dry hazard occurrences across the pan-Asian region

Davy Jean Abella, Kuk-Hyun Ahn *

Department of Civil and Environmental Engineering, Kongju National University, Cheon-an, South Korea

ARTICLE INFO

Keywords:
Climate extremes
Compound dry hazards
Cascading events
Pan-Asian region

ABSTRACT

Climate extremes have grown increasingly severe and frequent, posing significant threats to both economies and ecosystems. Prior research largely focused on individual hazard occurrences, often overlooking the compounded effects of multiple extreme events. With the escalating anthropogenic activities and increasing temperatures in Asia, there is an imperative need to investigate the occurrence of compound dry hazards (CDHs). This study aims to conduct a comprehensive assessment of CDHs in Asia, with a specific focus on examining the co-occurrence of heatwaves, droughts, fire dangers, and extreme winds over a 42-year period from 1980 to 2021. To be specific, our research focuses on evaluating interannual variability, identifying geographical hotspots, analyzing temporal shifts in cascading compound events, and exploring the dependence structure within CDHs. Our results indicate a significant increase in the spatial extent of CDHs in recent decades, with varying patterns in annual average frequencies across Asian regions. Particularly significant is the concentration of CDH hotspots within developing countries situated in East Asia, South Asia, and Southeast Asia. Moreover, our analysis highlights substantial increases in both the frequency and duration of cascading events (CEs), particularly in densely populated areas across North, Central, East, and West Asia. Conversely, South Asia experiences conspicuous declines in CEs. Lastly, our investigation into the dependence structure among CDHs illustrates varying degrees of interdependence among dry hazards and diverse spatial relationships across different Asian regions. We believe that these findings are highly valuable for enhancing natural risk management, improving climate model accuracy, and fortifying strategies to address the evolving risks associated with compound climate extremes under climate change.

1. Introduction

The frequency and intensity of climate extremes have witnessed a concerning rise in recent years, presenting a significant threat to both the environment and human society. The climate extremes, including hazards such as heatwaves, droughts, and storms, have prompted widespread consequences, leading to economic losses amounting to billions of dollars, habitat degradation, and loss of life (IPCC et al., 2022; Tavakol et al., 2020). Notably, since 1990, climate extremes have been responsible for approximately 1.6 million fatalities globally and an average annual economic loss ranging from USD 260–310 billion (Ward et al., 2020). In 2018, climate extremes impacted approximately 60 million individuals worldwide, resulting in the displacement of millions of people (Gu, 2019). Traditionally, the analysis addressing these extreme events has predominantly centered around examining them within a limited scope, concentrating solely on individual hazards. However, with a growing understanding of the interconnected nature of climate variables, it has become evident that solely examining individual hazards may lead to an inadequate assessment of the comprehensive impacts stemming from climate extremes, emphasizing the necessity of adopting a multi-hazard analysis (Kong et al., 2020; Leonard et al., 2014; Liu et al., 2022).

The co-occurrence of multiple extreme events, also known as compound hazards, have become more prevalent in recent decades (Mukherjee and Mishra, 2021; Tavakol et al., 2020; Yang et al., 2023). Several studies have shown its increasing frequency and impacts in many regions of the world. A study by the World Bank showed that a substantial portion of the global population has faced a high risk of exposure to compound hazards since 2005, with 105 million exposed to three or more concurrent hazards (Dilley, 2005). Particularly, the co-occurrence of heatwaves and drought has caused an average of 8 700 deaths per year from 2009 to 2019 worldwide (Ridder et al., 2022).

* Corresponding author.
E-mail addresses: davyabella@gmail.com (D.J. Abella), ahnkukhyun@kongju.ac.kr (K.-H. Ahn).

https://doi.org/10.1016/j.wace.2024.100669
Received 20 November 2023; Received in revised form 25 March 2024; Accepted 3 April 2024
Available online 4 April 2024

Meanwhile, coastal regions in Europe and the United States have experienced significant detrimental impacts of flooding, predominantly caused by the concurrent occurrence of storm surges and prolonged precipitation events (Paprotny et al., 2018; Wahl et al., 2015. On the other hand, Asian regions have suffered from intense heat and severe drought conditions in 2020, resulting in significant economic impacts across Southeast Asia. Countries such as Sri Lanka, Thailand, and Vietnam have been among the hardest hit. Indeed, the government of Thailand declared a state emergency due to drought-related saltwater intrusions into aquifers (Henson, 2020). With the changing global climate system due to human activities and the persistence of warming trends in various regions, more frequent and severe compound extreme events are expected in the future (IPCC et al., 2022; C. Wang et al., 2022; Yang et al., 2023).

To address the challenges posed by compound hazards, researchers have conducted numerous studies aimed at understanding their dynamics and developing effective strategies for mitigation and adaptation. Among the various co-occurring climate extremes under investigation, compounding dry hazards (CDHs), which pertain to simultaneous events caused by high temperature and low precipitation occurrences, have received significant attention (Sutanto et al., 2020). Traditionally, the analysis of CDHs has primarily focused on the co-occurrence of drought and heatwave (e.g., Liu et al., 2022; Mazdiyasni and AghaKouchak, 2015; Mukherjee and Mishra, 2021). However, recent studies have revealed that the simultaneous occurrence of the compound drought and heatwaves can also trigger other compound hazards, such as the occurrence of wildfire events (Libonati et al., 2022; Pu et al., 2022). Moreover, Evers et al. (2022) have shown that the occurrence of high-severity fires can also be influenced by the occurrence of extreme aridity. Previous studies have also addressed extreme winds as one of the components for dry hazard variables (Srock et al., 2018; N. L. Wang et al., 2022). Notably, extreme wind can potentially cause elevated evapotranspiration which could rapidly diminish soil moisture leading to the onset of flash droughts and increase fire risks (Leonard et al., 2014; Mass and Ovens, 2019; Zscheischler et al., 2020). These findings highlight the integral role of heatwaves, drought, fire dangers and extreme wind in defining CDHs and underscore the imperative for a comprehensive analysis of more than two co-occurring dry hazards (DHs) to fully address their impacts.

While acknowledging the significance of CDHs, it is noteworthy that the existing literature on investigating CDHs involving more than two events remains limited except for two studies (Sutanto et al., 2020; Yu et al., 2022). Sutanto et al. (2020) focused on assessing the co-occurrence of heatwaves, droughts, and fires in Europe, while Yu et al. (2022) explored patterns related to compound droughts, heatwaves, high temperature events, and wind events in Eurasian drylands. These studies have made valuable contributions by evaluating the spatiotemporal characteristics of CDHs, including identifying hotspots and analyzing occurrence regimes. However, these studies are still limited to understand the spatial evolution of CDHs, which is a relevant aspect in the multi-hazard impact assessment (Gill and Malamud, 2014). By expanding the analysis to incorporate the spatial dimension, we can expect to gain a deeper understanding of the interactions between different dry hazards. Therefore, exploring the interannual variability of the spatial extent and frequency of CDHs can provide valuable insights into understanding how the impacts of multiple DHs interact over time. This analysis stands as a distinctive contribution filling a crucial gap in the current understanding of CDHs.

Furthermore, the concept of cascading climate extremes (referred to as cascading events hereafter) is necessary to enhance the understanding of the interaction between multiple hazards (Depietri et al., 2018; Lawrence et al., 2020; Osman et al., 2022). The analysis of cascading events (CEs) takes into account multiple extreme events which occur sequentially or cumulatively without being disrupted by a no-hazard day (Yu et al., 2022). Previous literatures show that an initial hazard produces enough impact to cause subsequent hazards in the same area (e.g., AghaKouchak et al., 2018; Pescaroli and Alexander, 2018; Sutanto et al., 2020). For instance, Sutanto et al. (2020) found that drought is the most common precursor to the emergence of CEs, often leading to compound drought and fire occurrences. While promising, those studies have overlooked the temporal characteristics of CEs (e.g., maximum duration and frequency) and mainly focused on investigating the hazard patterns that may have triggered the chain effect of these events. While exploring the initial hazard or driver of a cascading event is crucial, neglecting its temporal characteristics may lead to underestimation of its underlying risks. By considering factors such as maximum duration and frequency, researchers can uncover critical insights into the duration and recurrence patterns of these events.

Recognizing the knowledge gaps in the literature, there is a clear need to explore the interconnectedness of compound dry hazards (CDHs) in a more comprehensive manner. This entails delving into the interannual variability of CDHs, encompassing both the spatial extent and frequency of their occurrence. By understanding how CDHs vary over time and space, we can identify hotspots where these hazardous conditions frequently occur and pinpoint areas of heightened vulnerability. Additionally, it is essential to investigate the dependence structure of CDHs and temporal characteristics of CEs to gain deeper insights into the dynamics and challenges associated with multivariate compounding hazards. Indeed, while some studies have provided notable insights in analyzing CDHs, their findings are predominantly limited to the multivariate analysis of DHs within the European and Eurasian drylands. However, the emerging extreme conditions associated with human activities, particularly compound dry and hot events, extend across a growing portion of land area, as highlighted by a recent report from the IPCC et al. (2022). Given that Asia is the most populous continent, accounting for approximately 60% of the global population as of 2023 (Population of Asia, 2023), and with millions of people being affected by drought and heat-related illnesses (WMO, 2022), it becomes increasingly crucial to evaluate the occurrence of CDHs within this region. Furthermore, the temperatures in Asia have been rising at a rate twice as fast as the global average (NOAA, 2021), further justifying the importance of such analyses to address the escalating risks.

In summary, the primary goal of this study is to conduct a comprehensive assessment of CDHs in Asia, specifically focusing on the co-occurrence of heatwaves, droughts, fire dangers, and extreme winds. To the best of the authors' knowledge, this approach has not been previously undertaken in the specific domain of our study, making it a valuable contribution to the understanding of these DHs and their interrelationships. We particularly employ a percentile-based threshold calculation method to identify the geographical occurrence of each hazard over a 42-year period from 1980 to 2021. To achieve the primary goal of this study, we address the following specific objectives:

1. Evaluating the interannual variability in both the spatial extent and frequency of CDHs in the entire Asia.
2. Identifying areas that serve as hotspots for the occurrence of CDHs.
3. Investigation of the significant temporal change in the frequency and duration of CEs within sub-regions of Asia.
4. Assessing the dependence structure that exists among the CDHs, exploring their interconnections and relationships.

The remainder of this paper is organized as follows. A description of the study area and data used are described in Section 2. Section 3 illustrates the methods used in defining the individual hazards and extracting CDHs. The details of the analysis of CDHs and their discussion are presented in Section 4 and Section 5, respectively. Finally, the paper concludes in Section 6 with a summary of the key findings and recommendations for future studies.

2. Study area and data

This study focuses on Asia, the largest continent in the world

covering approximately 30 percent of the Earth's land area. It is bordered by the Pacific, Indian, and Arctic Oceans which contributes to its unique weather patterns. It also exhibits a diverse range of climatic conditions influenced by various factors including geography, monsoons, and the interaction between land and ocean. Accordingly, Asia experiences a wide range of temperatures, with extreme variations between its northern and southern parts, leading to diverse susceptibilities to climate extremes. The northern regions of Asia have colder climates, influenced by the Siberian High and the Arctic air masses (Xu et al., 2019), whereas the southern regions have warmer climates influenced by tropical and subtropical air masses making them more vulnerable to intense heat extremes (Sharma et al., 2022; Wang et al., 2019). On the other hand, precipitation patterns in Asia are highly variable due to monsoons. While monsoonal rains bring substantial rainfall during specific seasons like the Indian summer monsoon and the East Asian monsoon, the region is also prone to periods of drought brought by global warming (Buckley et al., 2014). Along with the observed warming trends and increase in temperature across most of Asia, the residents' exposure to climate hazards are likely to intensify (Sharma et al., 2022). These shifts in weather patterns and increased exposure to climate extremes in Asia pose challenges for various sectors including agriculture, energy production, and human settlements, impacting their viability and adaptability (IPCC et al., 2022).

To facilitate the subregional assessment, the continent is divided into six sub-regions namely North Asia (NAS), Central Asia (CAS), West Asia (WAS), East Asia (EAS), South Asia (SAS), and Southeast Asia (SEAS). Fig. 1 illustrates the diverse Köppen climate classification across the subregions in Asia. North Asia is characterized by continental climates, marked by hot summers, cold winters, and significant temperature variations. Central and West Asia predominantly consist of arid regions where agriculture and water management face arduous conditions due to minimal rainfall and high temperatures. These regions in Asia are particularly vulnerable to wildfire and sandstorms which could threaten agricultural productivity and increase risks of desertification (Alizadeh-Choobari et al., 2016; Zittis et al., 2022). The Eastern and Southern parts of Asia are known for their climates characterized by hot, humid summers, and mild winters. Amidst the prevailing temperate conditions in these regions, the increasing frequency of extreme temperatures has also emerged as a recurring concern for the past decades (Sharma et al., 2022). Finally, Southeast Asia, characterized by its tropical climate, experiences high temperatures and abundant rainfall. While it has substantial precipitation that can support lush rainforests, there have been a growing concern of frequent drought occurrences in the region posing risks of water scarcity and affecting food security (Miyan, 2015). Given Asia's diverse climate conditions and its vulnerability to natural hazards, developing region-specific strategies is essential to address the

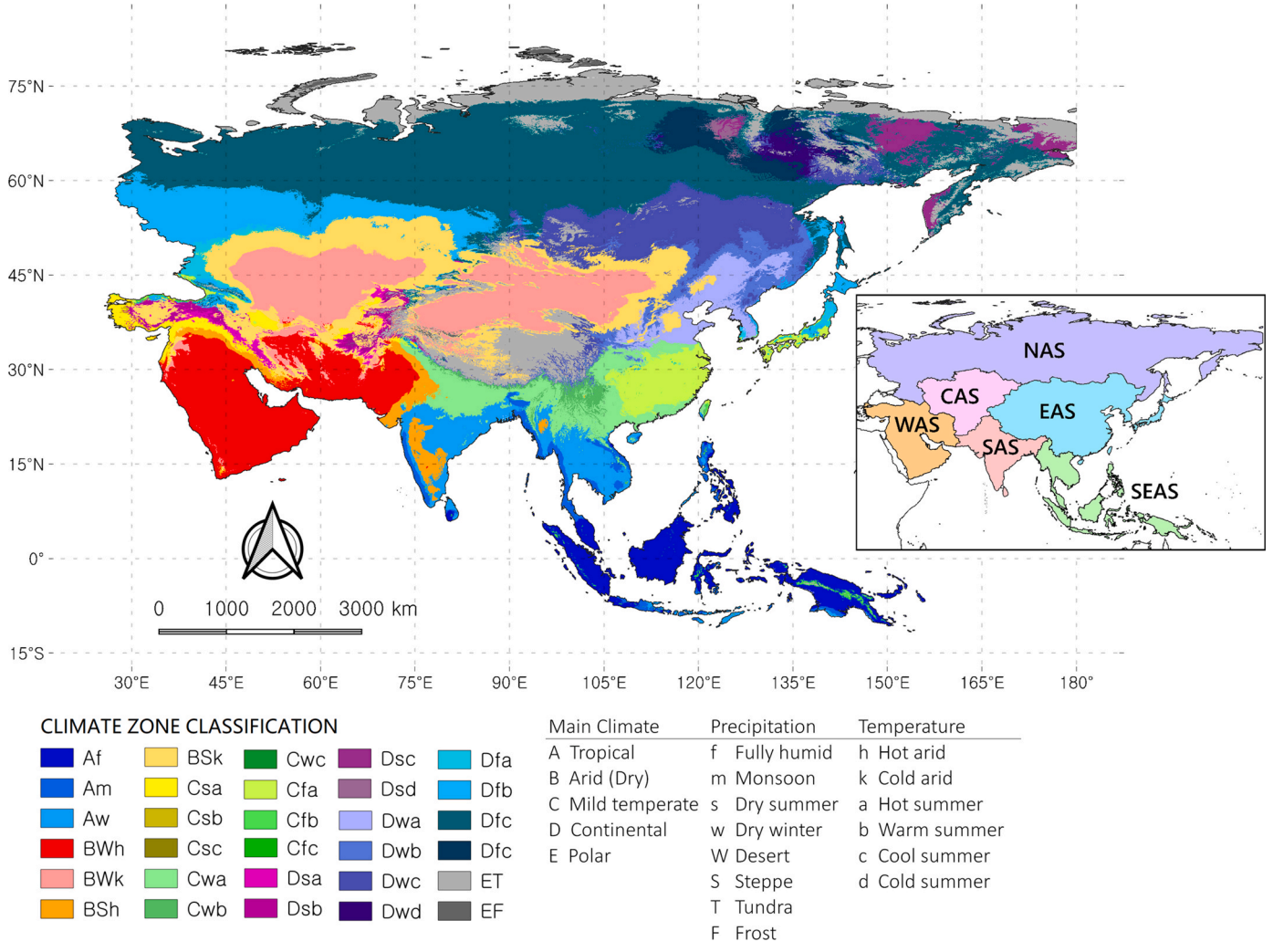

Fig. 1. The map of Asia showing the different climate zones categorized based on the Köppen Climate Classification. The Köppen system categorizes climates based on temperature and precipitation patterns, providing a comprehensive framework for understanding regional climatic variations. This classification aids in identifying and analyzing the climatic diversity across the Asian continent. The inset presents Asia divided into 6 subregions namely: North, Central, East, West, South and Southeast Asia.

continent's climatic challenges. Hence, a great deal of emphasis is also directed to the regional scale analysis of the occurrence of compound hazards in Asia.

This study utilized three climatological variables, including maximum temperature (T_{max}), total precipitation (P), zonal and meridional components of wind (W_s) for heatwave, drought, and extreme wind occurrences, respectively. Additionally, the Fire Weather Index (FWI) is utilized to assess the potential intensity of frontal fires. The FWI is a daily hybrid climate-weather index obtained by considering the impacts of fuel moisture, weather conditions, and an array of other factors influencing the likelihood and behavior of fires, thus aptly portraying potential fire risk (Van Wagner, 1987). These variables were obtained from the ERA5 reanalysis dataset, covering the entire Asia over the period of 42 years from January 1, 1980 to December 31, 2021. The ERA5 reanalysis dataset, provided by ECMWF (European Centre for Medium-Range Weather Forecasts), has been developed using the latest data assimilation methods and the most advanced numerical weather forecast model available, allowing for enhanced accuracy in estimating climatological variables (Hersbach et al., 2020). ERA5 has been widely utilized in characterizing extreme events in prior studies attesting its utility in capturing and representing climatological conditions (Aadhar and Mishra, 2023; Meng et al., 2023; Yu et al., 2022). Indeed, Jiao et al. (2021) and Lan et al. (2023) have reported that ERA5 is reliable in comparison to ground-based observations within the Asian domain. While the dataset is provided as hourly estimates with a spatial resolution of approximately 0.25° (~31 km) (Bell et al., 2021), we integrated the dataset into daily scales before conducting the analysis.

3. Methods

To assess the occurrence of CDHs, the methodology is described in three sections. First, we define individual hazard occurrences to generate daily binary maps for each dry hazard (DH) (Section 3.1). We then assess the spatial overlap of the daily binary maps to identify the occurrence of CDHs (Section 3.2). Lastly, a comprehensive set of analytical approaches aimed at investigating our research objectives (see Introduction) are presented in Section 3.3. A flowchart outlining the methodology is illustrated in Fig. 2.

3.1. Definition of individual dry hazards (DHs)

The methodology employed in defining each DH utilizes a threshold-based approach which involves analyzing the occurrences of climate variables (T_{max}, P, W_s) and FWI exceeding a specified threshold. These hazard thresholds are determined for each variable, ensuring consideration of their specific characteristics and requirements. A detailed

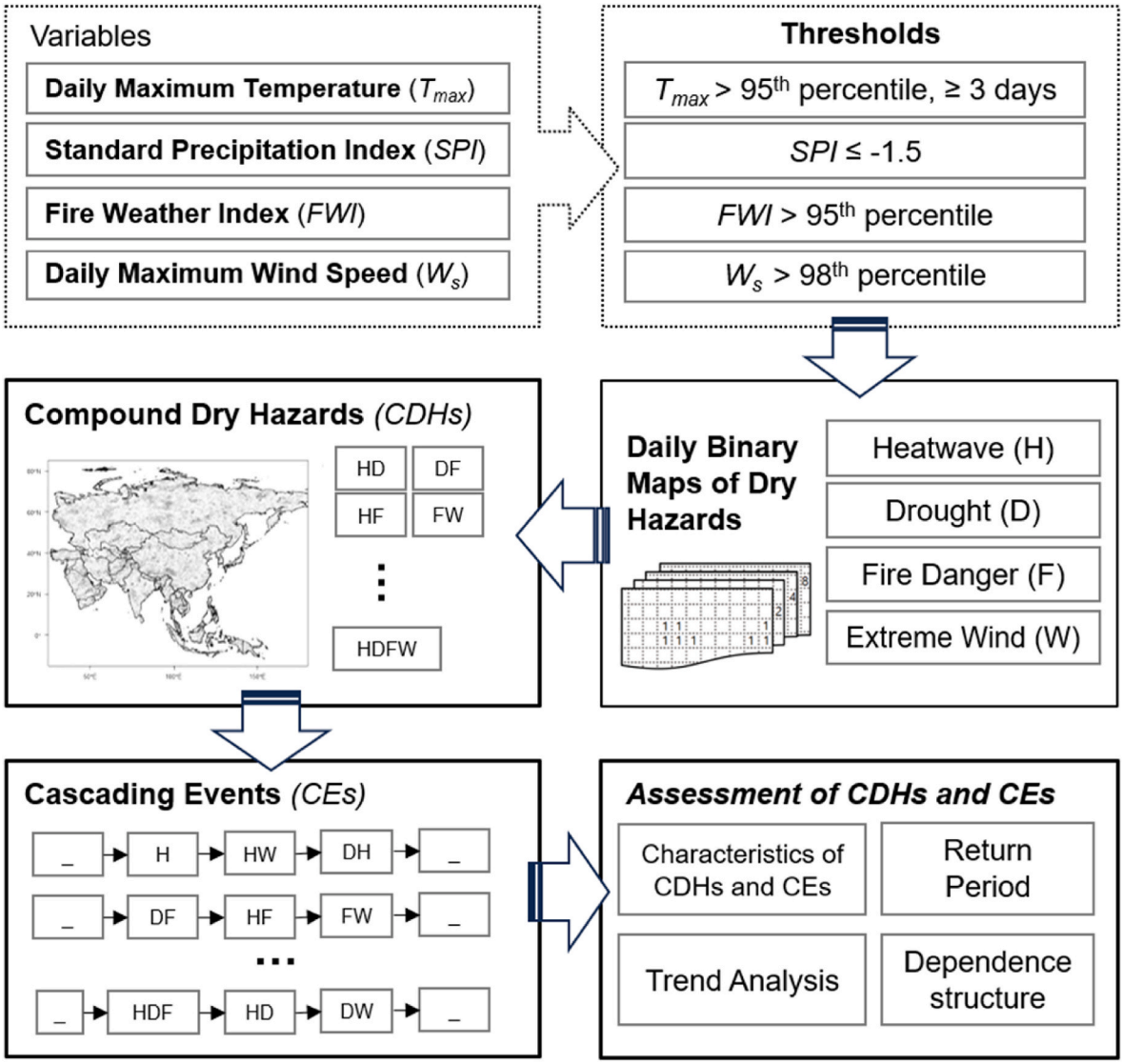

Fig. 2. Flowchart outlining the methodology adopted in this study.

description defining each DH and their thresholds is provided as follows.

3.1.1. Heatwave

While heatwaves are often characterized as prolonged periods of unusually high temperatures, a commonly accepted definition for a heatwave is yet to be established (Perkins-Kirkpatrick and Lewis, 2020; Shafiei Shiva et al., 2022). However, its identification often relies on surpassing a threshold based on climatological data for consecutive days (Ahn, 2022). This study also defines a heatwave event where the daily T_{max} exceeds the corresponding 95th percentile of the climatological distribution for at least three days. The selection of the specific percentile and minimum duration aligns with existing literatures on the subject (e.g., Baldwin et al., 2019; Stefanon et al., 2012). To calculate the climatological 95th percentile threshold, for each grid, we utilize the daily T_{max} within a 15-day moving window centered on each calendar day to smooth out any outliers or noises in the dataset. Accordingly, if the gridded dataset indicates the daily T_{max} exceeds the predefined threshold for a specific location and day, it is defined as a heatwave occurrence.

3.1.2. Drought

For drought characterization, we utilize the widely used Standardized Precipitation Index (SPI), which was initially proposed by McKee et al. (1993). The SPI employs cumulative precipitation data across diverse time frames (e.g., 30 days, 60 days, 360 days) to discern instances of drought events or unusual wetness patterns. It enables a more standardized evaluation of drought conditions across diverse geographical regions (Patel et al., 2007). This study particularly employs the cumulative precipitation time series on a 360-day timescale. This selection is made due to the suitability of the 360-day timescale in offering an extended, longer-term perspective on drought conditions (Russo et al., 2013; C. N. Wang et al., 2022). It is further supported by prior studies on drought assessment such as Das et al. (2020), Nosrati and Zareiee (2011) and Spinoni et al. (2014). These works have shown a preference for employing long-term time scales due to their effective presentation of drought patterns and capability to detect significant trends. Subsequently, the Standardized Precipitation Index (SPI) values are obtained by applying a probability distribution function to the cumulative data and then normalizing it to a standard normal distribution. In this process, we opt for the Gamma distribution, similar to previous research (e.g., Stagge et al., 2015; Zhang et al., 2023). Specifically, we classify occurrences as drought events when the SPI equals or drops below −1.50, serving as a marker for severe drought conditions.

3.1.3. Fire danger

To assess fire danger, we utilize FWI as a proxy of potential fire intensity given its robust empirical relationship in extreme fire events across diverse ecosystems (Abatzoglou et al., 2021; Semenova and Sumak, 2022). It is a comprehensive measure of fire intensity that incorporates factors representing the rate of spread and fuel consumption by combining the Initial Spread Index (ISI) and the Buildup Index (BUI). The FWI is computed using equations that convert ISI and BUI into the B-scale FWI and then into the S-scale FWI. It is expressed through the following equations (Van Wagner, 1974):

$$f(E) = \begin{cases} 0.626 \bullet BUI^{0.809} + 2, \text{for } BUI \leq 80 \\ \dfrac{1000}{25 + 108.64 \bullet e^{-0.023 \bullet BUI}}, \text{for } BUI > 80 \end{cases} \quad (1)$$

$$B = 0.1 \bullet ISI \bullet f(E) \quad (2)$$

$$FWI = e^{2.72\ (0.434 \ln B)^{0.647}} \quad (3)$$

where $f(E)$ is used to convert BUI into a measure of weight of fuel consumed; B is B-scale *FWI*; and *FWI* is the final S-scale *FWI*. However, for Eq. (3) when B is less than 1, *FWI* is simply set to B.

Fire danger can be classified based on a predefined threshold value of FWI. For instance, Good et al. (2008) and Herrera García et al. (2013) utilized FWI value of 30 in assessing the meteorological conditions associated with extreme fire danger. However, it has been observed that this classification may lead to over- or underestimation in various geographical regions with diverse climatic conditions (Varela et al., 2018). To circumvent this limitation, we opt for an alternative approach using a percentile-based threshold, akin to the methodologies employed in Dupire et al. (2017) and Goss et al. (2020). To be specific, this study identifies potential fire occurrence events when the FWI value at a particular location and day surpasses the 95th percentile threshold. This threshold is established for each grid cell, determined within a 15-day window centered on each calendar day spanning from 1980 to 2021.

3.1.4. Extreme wind

To characterize extreme winds, our approach involves the initial computation of hourly wind speed (W_s) magnitude. This computation is achieved by amalgamating the hourly 10-m zonal (v) and meridional (u) wind components, employing the formula $W_s = \sqrt{(u^2 + v^2)}$. The generated hourly W_s data is then aggregated into a dataset reflecting daily maximum W_s, which will serve as the basis for our analysis. In accordance with Martius et al. (2016), the 98th percentile threshold is considered as a damage-relevant wind threshold and focuses on extreme wind events significantly impacting large regions. Applying the identical process for assessing fire danger, we compute the daily 98th percentile for each grid cell, considering a window of 15 days centered around the given date. Extreme wind conditions are recognized when the W_s value exceeds the 98th percentile threshold on a particular day.

3.2. Definition of compound dry hazards (CDHs) and cascading events (CEs)

After identifying the spatiotemporal occurrence of each DH, we define CDHs by analyzing the spatial overlap of daily hazard maps. The initial step entails plotting the daily set of grid cells to their corresponding location to produce the daily hazard maps. These maps are then assigned specific values providing easier classification for each DH. To be specific, instead of utilizing a conventional binary map wherein each grid cell's attribute value is categorized as either zero (indicating an absence of hazard on that day) or one (indicating the presence of a DH), we use unique values to represent each DH. For example, the binary maps for heatwave and drought are represented by values 1 and 2, respectively. The selected values are ensured to produce distinct results after stacking. The stacking involves summing up the values per grid cell by spatially overlapping the daily binary maps of DHs. Thus, a resulting value of 3 following stacking signifies the co-occurrence of a compound heatwave and drought. The unique values assigned to each DH, along

Table 1
List of dry hazards (DH) and compound dry hazards (CDHs).

Value	Abb	Hazard(s)
0	–	No Hazard
1	H	Heatwave
2	D	Drought
3	HD	Heatwave + Drought
4	F	Fire
5	HF	Heatwave + Fire
6	DF	Drought + Fire
7	HDF	Heatwave + Drought + Fire
8	W	Wind
9	HW	Heatwave + Wind
10	DW	Drought + Wind
11	HDW	Heatwave + Drought + Wind
12	FW	Fire + Wind
13	HFW	Heatwave + Fire + Wind
14	DFW	Drought + Fire + Wind
15	HDFW	Heatwave + Drought + Fire + Wind

with the resulting value representing all potential CDH combinations, are provided in Table 1.

Following AghaKouchak et al. (2020), we characterize CEs as two or more hazards (DHs or CDHs) occurring consecutively or cumulatively without any interruptions. For the analysis of CEs, we explore diverse combinations of hazard sequences, each composed of a minimum of two distinct values (or one value for a compound hazard). In particular, we pay attention to the temporal continuity of both individual and compound hazards. As a result, accurately determining the beginning and end of a CE is of vital importance. Utilizing the spatiotemporal map of CDHs, we explore the CEs for each grid spanning the period from 1980 to 2021. Here, we overlay the daily CDHs maps and provide the necessary functions to analyze the frequency and duration of CEs. This process involves piling up all the daily hazard maps to generate the resultant map based on the inputted function. The beginning of a CE is determined when a DH or CDH value (refer to Table 1) is preceded by a zero value, indicating a no-hazard day. The CE continues until the sequence is disrupted by another zero value, marking the end of the event.

3.3. Assessment of CDHs and CEs

3.3.1. Characterization of CDHs and CEs

In this study, we first focus on the spatial extent and frequency of CDHs to evaluate its interannual spatial and temporal variability within a 42-year period from 1980 to 2021. The annual spatial extent of CDHs is obtained by calculating the ratio of the number of grid cells with CDHs for each year to the total number of grid cells over Asia. For the annual occurrence frequency, we calculate the average frequency for each CDH combination per year across all grids within the six subregions in Asia.

Next, we characterize CEs in three aspects including the average frequency of events, maximum duration, and average duration. For each grid, we define the average frequency as the total number of uninterrupted DHs and/or CDHs sequences divided by the number of years over the study period. The maximum duration is defined as the highest number of DHs and/or CDHs occurrences observed among all CEs. Lastly, the average duration is calculated by summing the durations of all CEs and dividing the total by the frequency of events. To gain a comprehensive understanding of CEs across diverse climate conditions, both pan-Asia and regional-based analysis are performed in this study. This regional perspective facilitates an investigation into unique attributes and trends of CEs within various climatic zones.

3.3.2. Return period

Areas that serve as hotpots for the occurrence of CDHs are determined based on its return period. Return period ($\mathscr{R}$) is defined as the average time interval between recurrences of extreme events. Here, $\mathscr{R}$ is calculated from the joint occurrence probabilities ($\mathscr{P}$) of each CDH following Yu et al. (2022). For each grid cell, $\mathscr{P}$ is calculated by determining the ratio of the number of days in which a CDH occurs (n) to the total number of days during the period 1980–2021 (N = 15341 days). The value of $\mathscr{R}$ is then obtained as the inverse of joint occurrence probability and dividing the result by 365 to obtain a unit of years. The equations for $\mathscr{P}$ and $\mathscr{R}$ are as follows:

$$\mathscr{P} = \frac{\sum_{i=1}^{n} CDH_i}{N} \tag{4}$$

$$\mathscr{R} = \frac{1}{\mathscr{P} \times 365} \tag{5}$$

where, CDH_i represents the occurrence of a compound dry hazard on the specific i^{th} day. A small $\mathscr{R}$ value indicates a higher likelihood of an event occurring more frequently. Thus, hotspots for CDHs are characterized as regions with smaller $\mathscr{R}$ values, implying a high frequency of CHDs.

3.3.3. Trend analysis

This study uses the widely used nonparametric Mann-Kendall trend test (Kendall, 1948; Mann, 1945) to assess the statistical significance of monotonic trends of CDHs (i.e., spatial extent and frequency) and CEs (i.e., frequency and duration) throughout Asia. the MK test statistic (S) is calculated as follows:

$$S = \sum_{k=1}^{m-1} \sum_{j=k+1}^{m} sgn(x_j - x_k) \tag{6}$$

where $sgn(x_j - x_k) = +1$ if $x_j > x_k$; $= 0$ if $x_j = x_k$; $= -1$ if $x_j < x_k$; x_j and x_k are the values of sequence j, k; and m is the length of the time series. Then, the standardized test statistic (Z) is calculated by:

$$Z = \frac{S \pm 1}{\sqrt{var(S)}} \tag{7}$$

This equation uses S-1 if $S > 0$, S+1 if $S < 0$, and Z is 0 if $S = 0$. If Z is greater than 0, it indicates an increasing trend, and vice versa. The trends are evaluated with a confidence level of 95%. Besides, the magnitude of a time series trend is estimated using a non-parametric procedure developed by Sen (1968). The trend is calculated by

$$\beta = Median\left(\frac{x_j - x_k}{j - k}\right), j > k \tag{8}$$

where $\boldsymbol{\beta}$ represents Sen's slope estimate. A positive $\boldsymbol{\beta}$ value indicates an upward trend in the time series, while a negative value suggests a downward trend during the specified time period.

3.3.4. Dependence structure among CDHs

To assess the dependence structure that exists among CDHs, this study utilizes the likelihood multiplication factor (LMF) introduced by Zscheischler and Seneviratne (2017). Ridder et al. (2020) have also utilized LMF to illustrate the impact of the possible correlation between hazard pairs on the joint occurrence probability. Although correlation analysis can yield a similar inference, the LMF holds a distinct advantage as it can be employed to multidimensional hazards, allowing for a comprehensive understanding of their overall interdependence. Here, LMF is defined as the ratio of the joint occurrence probability of a CDH ($\mathscr{P}$) and the probability assuming complete independence between a CDH combination ($\mathscr{P}_{indep}$). Following the approach of Ridder et al. (2020), the LMF for each CDH combination (e.g., HD, DF, HDW, DFW, and so on) is calculated for each grid cell individually and can be expressed as follows:

$$\mathscr{P}_{indep} = \prod_{h=1}^{H} \mathscr{P}(\mathrm{DH})_h \tag{9}$$

$$LMF = \frac{\mathscr{P}}{\mathscr{P}_{indep}} \tag{10}$$

where h is the indicator of a particular DH; and H is the total number of DH presented in a CDH. The LMF varies between 0 and infinity. For positively correlated hazard pairs, the LMF exceeds 1, while the LMF lies between 0 and 1 for negatively correlated hazards.

4. Results

4.1. Interannual variability of spatial extent and frequency of CDHs

Initially, the study examines the interannual variation in the spatial extent of CDHs over the period from 1980 to 2021. Fig. 3 shows the percentage of areas covered by each of the CDH type each year across Asia, along with the trend slope and its corresponding 95% confidence interval. Overall, there has been a substantial surge in the occurrence of CDHs during this period with an increasing trend ranging from 0.004%

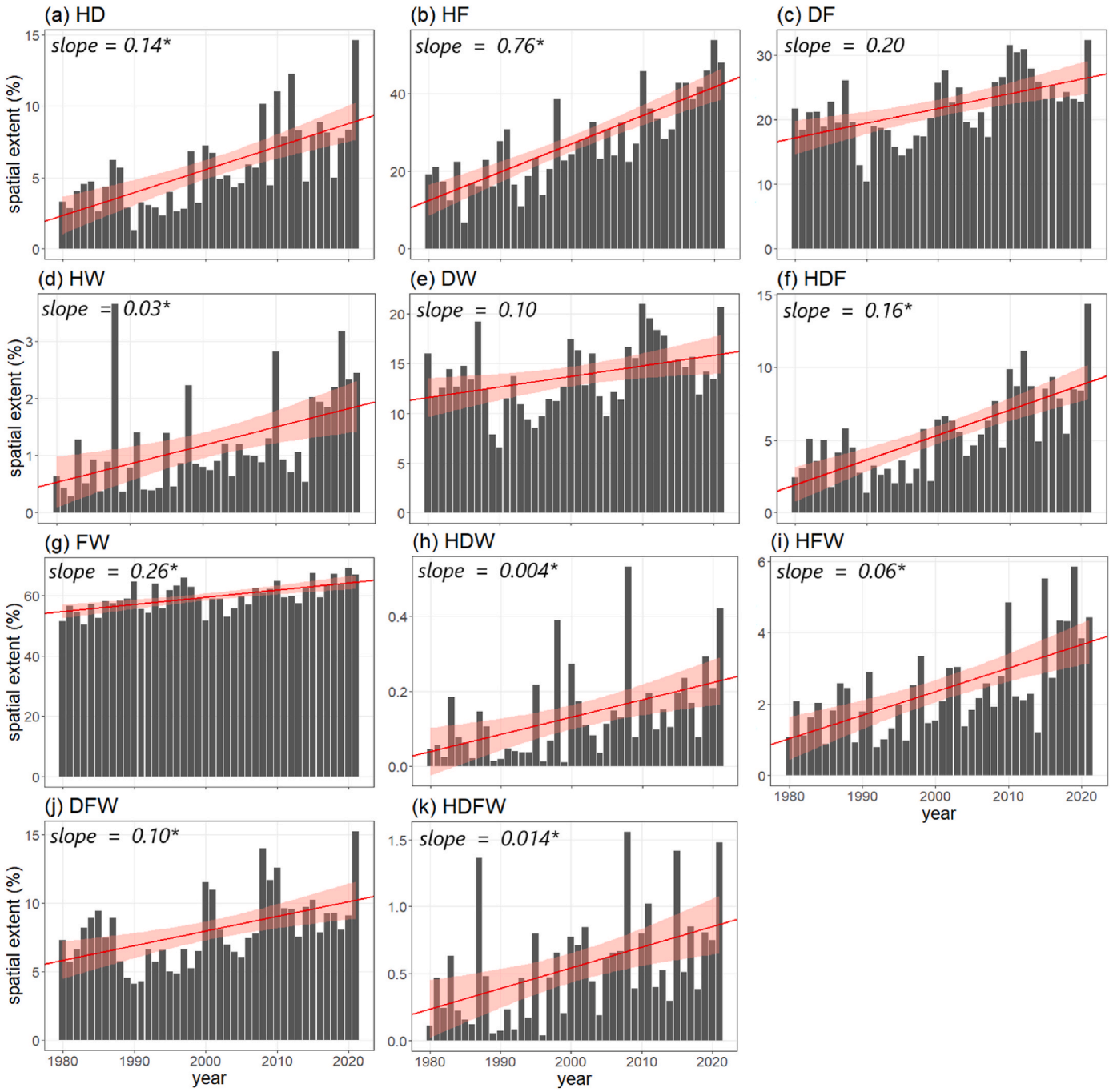

Fig. 3. The annual percentage of areas in Asia covered by each compound dry hazard (CDH) combination from 1980 to 2021. Each combination shows the interannual variability of the spatial extent of occurrence of CDHs in the entire Asian region. The slope (red line), confidence interval (red bandwidth) and magnitude of trend (*slope*) are also presented. *slope* values with asterisk (*) indicate significant trends (*p-value* < *0.05*). The slope of the trends show an increase of CDHs occurrence where all dry hazard combinations excluding DF and DW have shown significant upward trends. (For interpretation of the references to color in this figure legend, the reader is referred to the Web version of this article.)

to 0.76%. Among the CDHs, results show that HF (Fig. 3b) exhibited the highest significant increase (*p-value* < 0.05) in spatial extent covering less than 20% of Asia in 1980, but by 2021, it has expanded to more than 40% of the region. Following HF is FW (Fig. 3g) which showed a significantly increasing trend of 0.26% while other CDHs also demonstrated a considerable rise in the spatial extents over the same period. In total, the eight combinations of CDHs including HD, HW, HDF, HDW, HFW, DFW, and HDFW show significant increases. While DF (Fig. 3c) and DW (Fig. 3e) did not show significant trends, it still exhibited an observable increase in spatial extents within the recent decades. Moreover, HD, HDF, HDW, DFW, and HDFW have showed concerning signs of rapid emergence as their spatial extent surges rather abruptly in 2021. Meanwhile, decreases in spatial occurrence of most CDHs are observed in the period 2012–2018. Despite this, the spatial extent of CDHs in this period continuously exhibit a higher percentage of spatial extent compared to the preceding decades. Indeed, most of the high percentage of the extent of CDHs in Asia is observed between 2019 and 2021. Overall, the consistent upward trend in the spatial extent of CDHs clearly illustrates the growing impact of compound dry hazards in recent decades.

Fig. 4 presents the annual average frequency (days/grid cell) of CDHs from 1980 to 2021. Since Asia has a massive area with diverse geographical characteristics, this assessment is conducted on a regional scale. Among the CDHs, DF stands out with the highest average occurrence and its prevalence extends across all the Asian sub-regions. Results also highlight substantial variation in the yearly average frequency of DF with pronounced peaks occurring in various time intervals between 1980 and 2021. Particularly, in EAS (Fig. 4c), DF peaked in the years 1984 and 2008–2009 with an average frequency of approximately 15 days. In SEAS (Fig. 4f), the highest average frequency of DF is approximately 14 days which occurred during the years 1998–1990. For the rest of the subregions in Asia (i.e., NAS, CAS, WAS, and SAS), the highest average frequency of DF is observed in 2021. Meanwhile, other CDHs exhibited relatively modest year-to-year changes in contrast to DF within each subregion. However, certain noteworthy points have been identified. For instance, in NAS (Fig. 4b), the increase of average frequency of HDF and HF is evident for the past decade. Its increasing trend started around 2005 and peaked in 2010 then decreased and increased again after a few years. Similarly, for CAS (Fig. 4a) and SAS (Fig. 4e), decadal fluctuations for HD, HDF and HW are observed. Although DF is prevalent in all regions in Asia, results of CDHs in each subregion showed a varying pattern suggesting the influence of the diverse geographical characteristics in the frequency of CDHs.

4.2. Hotspots of CDHs

The hotspots of CDHs are defined as geographical regions with short return periods in the joint occurrence of a specific hazard combination (see Fig. 5: hotspots are indicated in red color). Among the CDHs, DF (Fig. 5c) has the least average return period and is widespread in entire Asia with approximately 5% and 60% of the area have a return period of 0.25 and 0.5 years, respectively. Hotspots of DF include the Tibetan Plateau and northeastern part of China, and widespread across Southeast Asia. Meanwhile, the occurrence of HW (Fig. 5d) is relatively low compared to other hazard pairs and is observed in most regions in East Asia and Southeast Asia. While most the of CDHs involving two hazards are frequently observed throughout Asia, the occurrence of HW has a minimum return period of 4 years. Hotspots of HD (Fig. 5a) is prevalent along the South Asian region, the northern part of Southeast Asia, and lower regions in East Asia with return periods of approximately less than two years. While HD covers most of the region in South Asia, a more frequent occurrence is observed in the southeastern part of East Asia (i.e., Guangdong, China). Hotspots of HF (Fig. 5b) are concentrated in Southeast Asia and South Asia where the return period is approximately 0.25 years. Additionally, HF occurs in more than 50% of Asia (prevalently in North and East Asian regions) where return period is approximately 0.50–2 years. The rest of the continent particularly most of the West Asian region, northwestern part of China, and southern part of Central Asia have a return period of more than 2 years. In contrast, the return period of FW (Fig. 5g) is at most 1 year and its hotspots extend throughout West Asia with higher incidence in Saudi Arabia. It can also be observed that FW is most prevalent in regions in Asia with arid climate (refer to Fig. 1) which include the lower regions of Central Asia and northern parts of East Asia. On the other hand, hotspots of DW

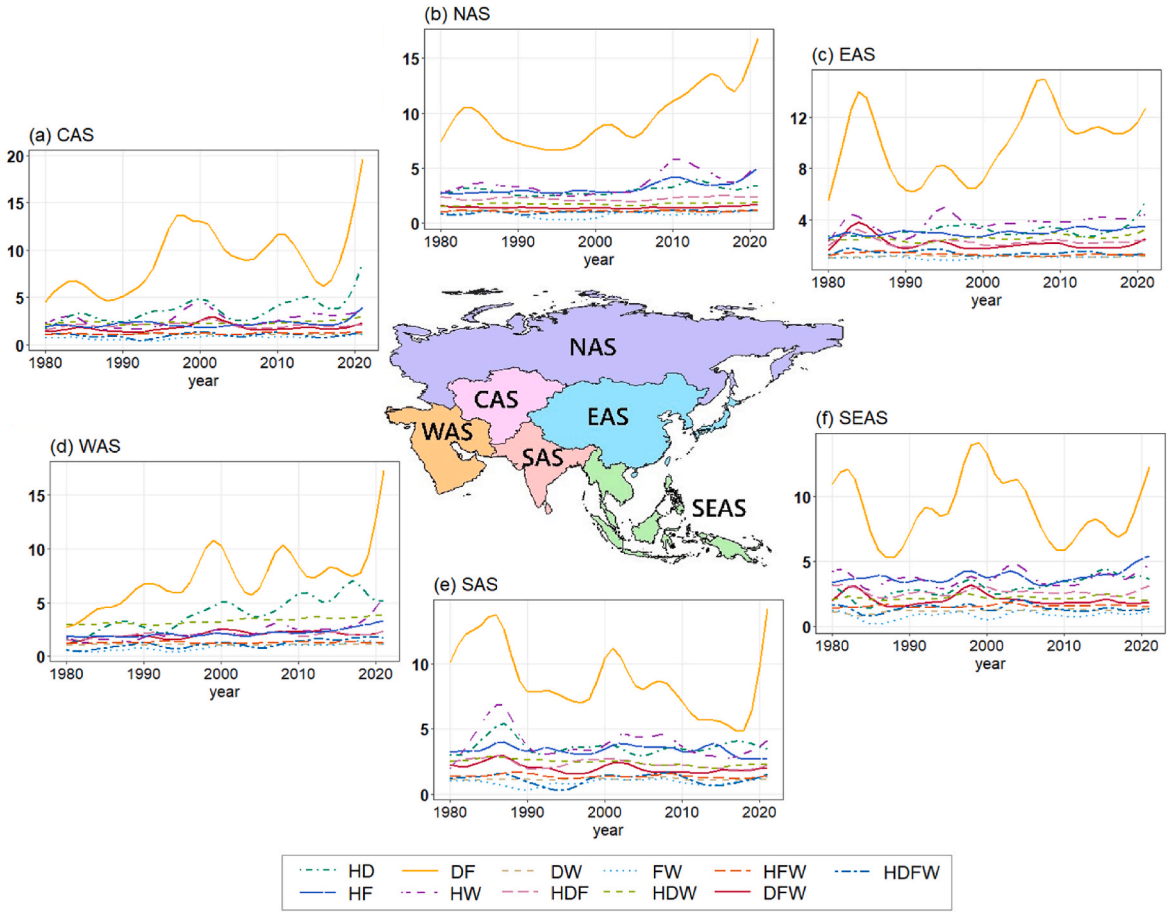

Fig. 4. Annual average frequency (days/grid cell) of compound dry hazards across six distinct subregions in Asia from 1980 to 2021. Subregions include (a) Central Asia, (b) North Asia, (c) East Asia, (d) West Asia, (e) South Asia, and (f) Southeast Asia. The legend provides abbreviations for various compound dry hazards, as detailed in Table 1. Lines are fitted using the smoothing spline technique to highlight the underlying patterns of annual average frequency within each region, aiding in the visualization and interpretation of climatic trends over the past decades.

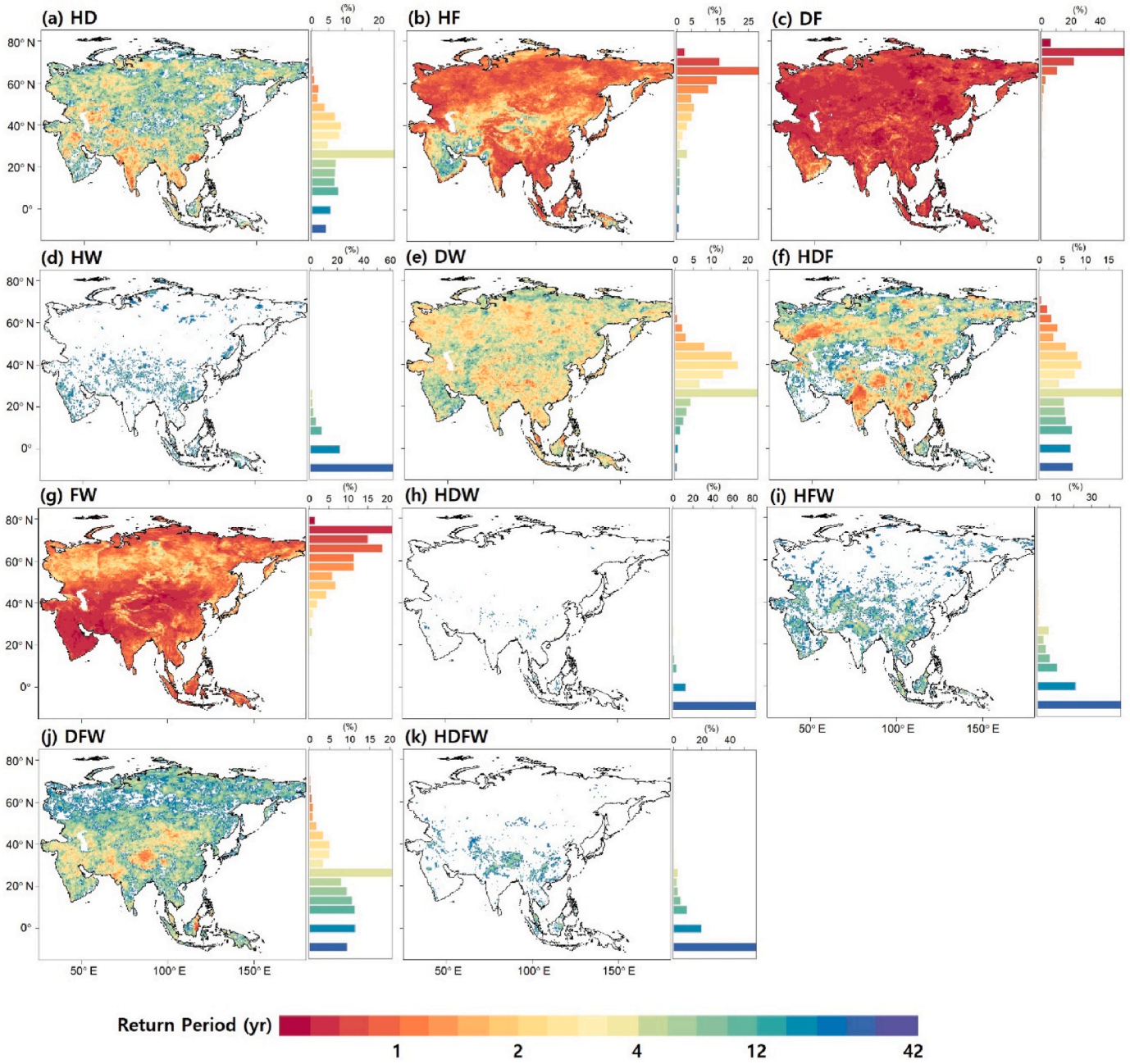

Fig. 5. Return periods of compound dry hazards (CDHs) in Asia (hotspots are indicated in red color). The horizontal histograms adjacent to each map represent the percentage (%) distribution of return period intervals for each CDH occurrence. Definitions of each CDH combination are indicated in Table 1. (For interpretation of the references to color in this figure legend, the reader is referred to the Web version of this article.)

(Fig. 5e) are observed in Southwest China, Malaysia and northern part of Indonesia.

Among the CDHs simultaneously involving three to four hazards, HDF (Fig. 5f) stands out as it exhibits the most extensive spatial coverage and frequent occurrences. Hotspots of HDF are observed in diverse areas such as the western districts of Russia, the northern regions of India, the southern parts of China, and scattered regions across Southeast Asia with return period of 0.25–0.50 years. Hotspots of DFW are observed in the Tibetan Plateau and in Indonesia. The occurrence of HFW and HDFW are mostly observed in the lower regions in Asia with return period that ranges from 3 to 4 years. Meanwhile, HDW has the least occurrence among the compound hazards mentioned with return period of more than 12 years and is observed across the East and Southeast Asian regions. When considering the entirety of Asia, the subregions most significantly affected by CDHs encompass East Asia, South Asia, and Southeast Asia. The prevalence of CDHs in these regions is further explored in Section 5. Overall, these findings highlight the distribution and varying frequency of CDHs, providing crucial insights into the geographical areas that are particularly vulnerable to the combined impacts of these DHs.

4.3. Temporal change in frequency and duration of CEs

In this section, we examine the characteristics of CEs in Asia encompassing the average frequency of CEs (Fig. 6a), maximum duration (Fig. 6b), and average duration (Fig. 6c). The occurrence of CEs spans a substantial portion of Asia, with average frequencies ranging between four and seven CEs per year (average annual frequency of

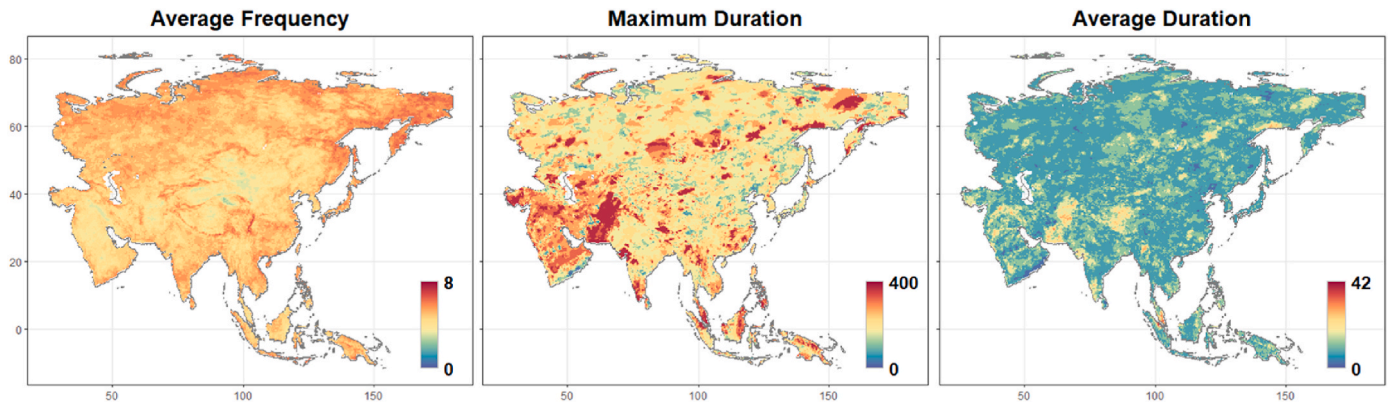

Fig. 6. Characteristics of cascading events (CEs) in Asia defined based on (a) average frequency of CEs, (b) maximum duration (days) of CEs, and (c) average duration (days) of CEs for the past 42 years from 1980 to 2021.

cascading events, in days per grid cell, in entire Asia is also shown in Fig. S4). High maximum and average duration of CEs, on the other hand, are observed in scattered regions across the continent. Specifically, the results indicate that the occurrence of frequent CEs in Asia is most prevalent in the northern region, particularly concentrated in the western districts of Russia. Frequent events are also evident in Japan and the Philippines. Over a span of 42 years (1980–2021), an average of at least 6 events per year have been observed in these regions. In contrast, a large part of West Asia, along with Afghanistan and the northern regions of East Asia, emerges as an area with less frequent CEs. However, a noteworthy contrast can be observed when examining Fig. 6b when compared to Fig. 6a. Most regions characterized by lower average occurrence of CEs often experience prolonged duration for these events. Longer duration of CEs are also evident in Southeast Asia particularly in the Philippines, Malaysia, and Indonesia. Meanwhile, higher average duration of CEs (Fig. 6c) is prevalent in Afghanistan, indicating that frequent prolonged durations of CEs are experienced in these regions.

Next, the temporal change in the frequency and duration of CEs are

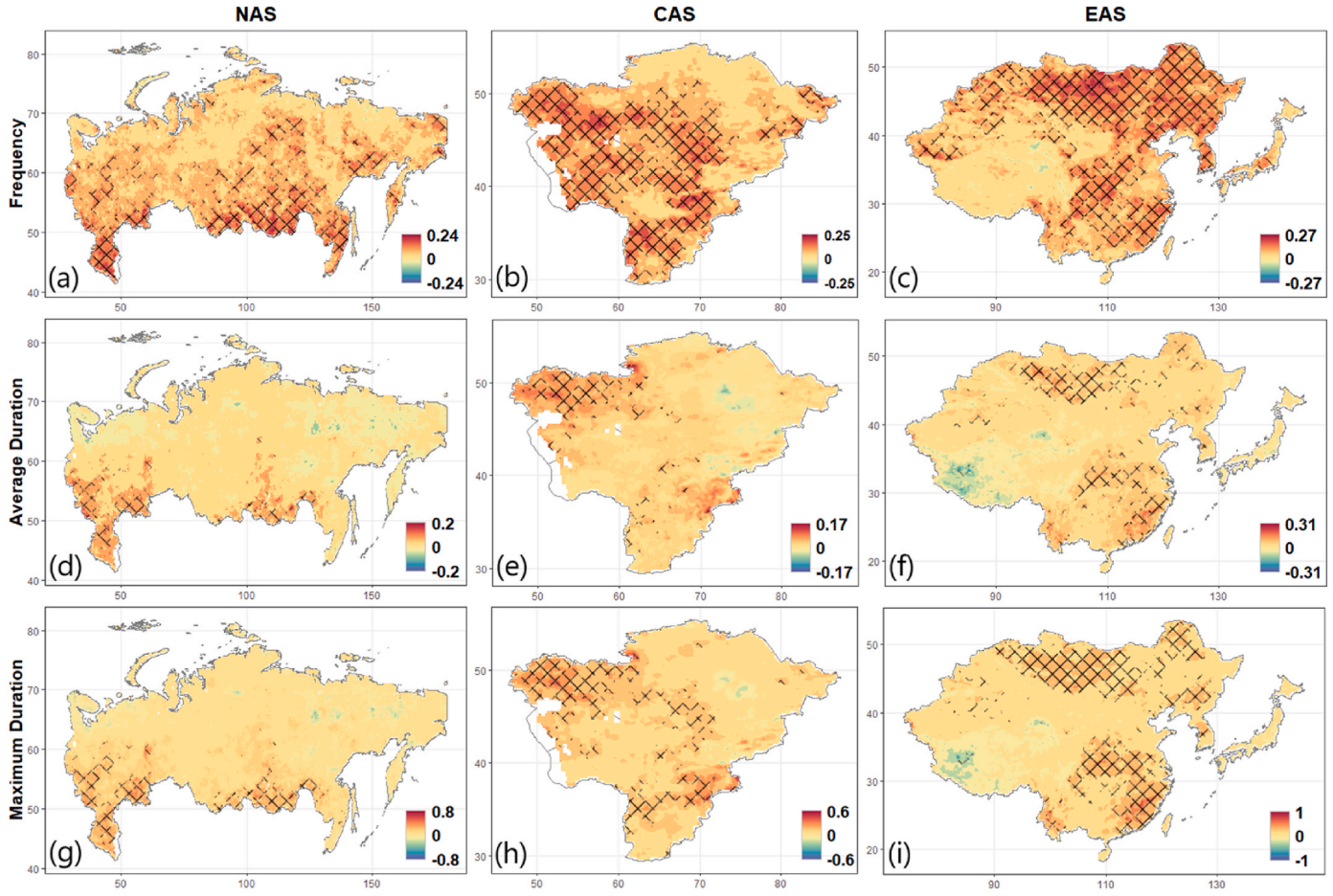

Fig. 7. Results of regional-scale trend analysis for North Asia (NAS), Central Asia (CAS), and East Asia (EAS) using Sen's slope method. The analysis examines trends in the frequency (a–c), average duration (d–f), and maximum duration (g–i) of cascading events over a span of 42 years, from 1980 to 2021. Significant trends, identified with a 95% confidence interval, are represented by stippling. Additionally, redder areas on the map indicate an increase, while bluer areas indicate a decrease in the occurrence of compound dry hazards across these regions.

evaluated from the regional scale trend analysis presented in Fig. 7 (for NAS, CAS, and EAS) and Fig. 8 (for WAS, SAS, and SEAS). Results indicate an increasing trend in the frequency of CEs in most regions of Asia. A widespread significant increase in frequency is evident in NAS, CAS, and EAS (see Fig. 7a–c). Meanwhile, substantial increasing trends in average duration of CEs (Fig. 7d and e) are concentrated in specific regions including the lower regions of NAS (i.e., Southern Russia and southern portion of Siberia), and northwest part of CAS (i.e., West Kazakhstan Region). For EAS (Fig. 7f), Mongolia, Central and South China Districts are observed to have pronounced increases while certain areas in Tibetan Plateau exhibit moderate to significant decrease in average duration. Similarly, notable trends in maximum duration (Fig. 7g–i) are identified in the same areas where pronounced trends of average duration are observed.

While NAS, CAS, and EAS display a consistent increasing trend across the regions, Fig. 8 exhibit diverse patterns of increasing and decreasing trends throughout WAS, SAS, and SEAS. Particularly, it is apparent that nearly the entire region of WAS underwent a significant increase in the frequency of CEs (Fig. 8a). Substantial trends of increasing average CE duration in WAS are visible in scattered regions across Turkey, Saudi Arabia, and Iran (Fig. 8d). A similar pattern is observed in the maximum duration of CEs, but with a more extensive coverage across these regions (Fig. 8g). In contrast, Fig. 8b highlights a significant decline in CE frequency, particularly evident in the majority of the SAS region, especially Central India, and more prominently in Southern Pakistan. It is also noted that the northwestern region of Pakistan presents a significant increase in CE frequency. Similarly, Furthermore, Fig. 8e and h exhibit both upward and downward trends in the average and maximum duration of CEs in SAS. Increasing trends are concentrated in the northern regions, while decreasing trends are observable in the central area of SAS, albeit to a lesser extent. Additionally, frequency of CEs in SEAS (Fig. 8c) suggests widespread substantial rise in countries including Laos, Vietnam, and Indonesia. However, despite the widespread increase of frequency of CEs throughout the region, only a small area displayed notable increasing trends in the average (Fig. 8f) and maximum duration (Fig. 8i) of CEs. Affected countries include Cambodia, Indonesia, and northern regions of Myanmar. In summary, the analysis of characteristics and trends of CEs in Asia reveals distinct patterns of frequency and duration across various regions. This observation also motivates us to further explore the relationship of CDHs which will be addressed in the following section.

4.4. *Dependence structure among CDHs*

Fig. 9 exhibits the dependence structure among CDHs in Asia. Intriguingly, our analysis showed that the relationship among the selected independent variables of CDHs (i.e., heatwave, drought, extreme winds, and fire) exhibit varying degrees of interdependence. Notably, our results reveal instances where certain combinations of these variables exhibit strong positive correlations such as HF, FW, DF, HDF, and DFW that span extensively across Asia, highlighting the synergy between dry hazard occurrences. For instance, HF exhibits a robust positive correlation (Fig. 9b), indicating that heatwave conditions often coincide with increased fire risks. However, other combinations may

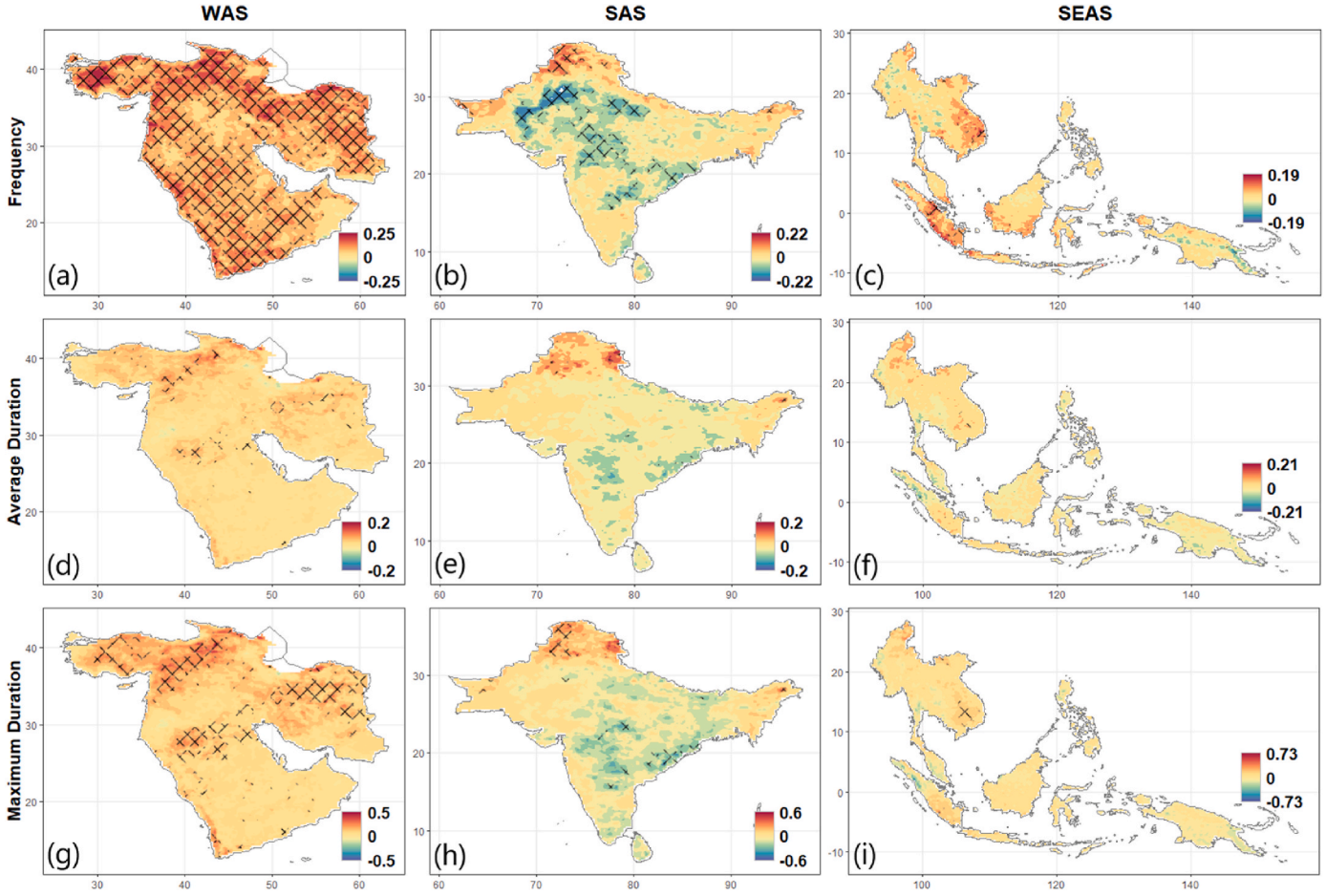

Fig. 8. Results of regional-scale trend analysis for West Asia (WAS), South Asia (SAS), and Southeast Asia (SEAS) using Sen's slope method. The analysis examines trends in the frequency (a–c), average duration (d–f), and maximum duration (g–i) of cascading events over a span of 42 years, from 1980 to 2021. Significant trends, identified with a 95% confidence interval, are represented by stippling. Additionally, redder areas on the map indicate an increase, while bluer areas indicate a decrease in the occurrence of compound dry hazards across these regions.

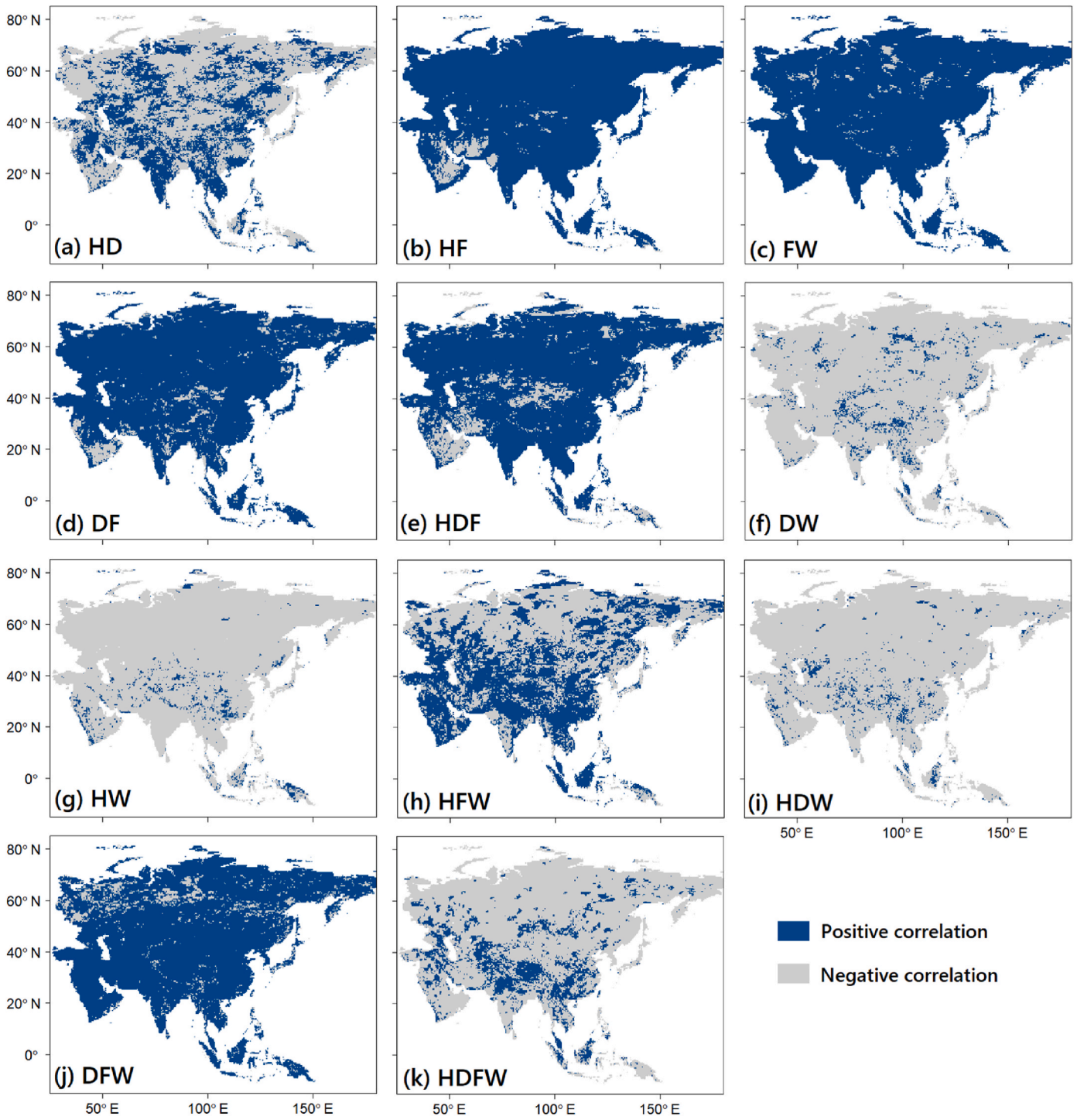

Fig. 9. Dependence structure among CDHs obtained from likelihood multiplication factor (LMF) analysis. LMF values are categorized into two: positive (blue) and negative (gray) correlations to provide a direct perspective on their underlying relationships. (For interpretation of the references to color in this figure legend, the reader is referred to the Web version of this article.)

demonstrate weaker correlations. For example, when compared to HF, the correlation between HW is less pronounced (Fig. 9g), suggesting that heatwaves do not necessarily align with strong wind conditions. Similarly, DW does not display a substantial correlation even on a regional scale (Fig. 9f), indicating that the occurrence of drought does not entirely influence the likelihood of extreme winds or vice versa. However, an interesting observation arises when DW coincides with fire (i.e., DFW). It leads to a compelling positive correlation that spans across nearly the entire Asian continent (Fig. 9j). This may be attributed to the dry vegetation resulting from drought, which becomes highly susceptible to ignition, and the presence of wind which can accelerate the spread of fires, which is also found in the previous studies (e.g., Littell et al., 2016). This also aligns with the positive correlations exhibited in other fire-related CDHs such as FW (Fig. 9c) and DF (Fig. 9d), indicating that the conditions conducive to fires are often accompanied by the presence of other DHs as well.

Additionally, it is noteworthy to emphasize that despite some CDHs showing negative correlations in most regions, positive relationships can

be observed in localized areas. For example, positively correlated CDHs involving HD, HW, HFW, HDW, and HDFW are more pronounced in lower latitude regions of the continent, albeit in minimal extents. Similarly, despite the prevalence of positive relationships of CDHs such as HF, FW, DF, HDF, and DFW, certain regions across the continent still exhibit a negative correlation. These variations may be attributed by local characteristics that could impose constraints or amplify the relationships between specific CDHs. In summary, our analysis demonstrates that a range of dependencies among CDH variables are observed, with certain combinations exhibiting particularly strong relationships.

5. Discussion

This study investigates the co-occurrence of multiple dry hazards (DHs), providing a more comprehensive view of complex interactions among multiple extreme events. However, we note that our investigation did not delve into the specific drivers of CDHs. Instead, we focused on the assessment of the significant spatial and temporal characteristics among the CDHs. Our exploration of the interannual variability in CDH's spatial extents highlights a significant and widespread surge in CDH occurrences throughout Asia over the recent 42 years. Also, trends in CEs mostly exhibit an increase across the subregions, underscoring the escalating influence of the CDH events. However, mixed anomalies can still be observed in various regions. It informs that additional factors beyond the generalized trends might contribute to the multifaceted nature of CDH occurrences. This can also be further justified by the varying hotspots of CDHs in Asia which suggests that the diversity in local conditions across different regions significantly influences the prevalence and characteristics of these CDHs.

This study shows a compelling interconnected relationship among various DHs that collectively contribute to the widespread increase of CDHs. In particular, prior research has indicated that the escalation of CDHs can be attributed to heatwaves causing high evaporation rates, resulting in soil desiccation, which in turn heightens vegetation dryness and flammability (Afroz et al., 2023; Silva et al., 2022). As an illustration, the considerable spatial coverage of HD (Fig. 3a) in both 1997 and 2010 could be linked to the variations in the elevated percentage of HF (Fig. 3b) during those corresponding years. It informs a synergistic relationship between drought, fire, and the concurrent presence of heatwaves. Similarly, Evers et al. (2022) and Abram et al. (2021) proposed a strong likelihood of fires occurring during periods when drought and extreme winds coincide. In this study, even though DW (Fig. 3e) did not exhibit a significant increase, the simultaneous peak occurrence of DFW (Fig. 3j) and DW in the same years implies a close association between extreme winds and fire hazard. These spatial connections between heatwave-induced soil desiccation and fire hazards or wind-driven fires underscore their interdependence, providing valuable insights to understand the potential mechanisms influencing CDH occurrences. Nevertheless, our study primarily focuses on the exploration of the temporal and spatial occurrence of CDHs and did not extensively examine the individual risks or impacts associated with each CDH. Indeed, not all dry hazard combinations could potentially lead to adverse outcomes such as the simultaneous or cascading occurrences of HW and DW. For instance, the presence of extreme wind following a drought may not directly trigger significant risks. However, its simultaneous occurrence could still potentially serve as precursors to subsequent compound events. Prioritizing research on the specific drivers of CDHs and their implications would be a promising avenue for future work.

The hotspots of CDH occurrence specifically East Asia, South Asia, and Southeast Asia can be attributed to a combination of various regional factors involving regional climatic conditions and transformations in land use practices (IPCC et al., 2022). For example, regions significantly affected by heatwave and fire events often encompass low-latitude areas characterized by tropical and arid climates (refer to Fig. 5). This alignment suggests that specific climatic conditions significantly contribute to the occurrence of such events. Notably, the spatial distribution of HD, HF, and DF events demonstrates a remarkable degree of similarity when compared with both regional and global outcomes (e.g., Ridder et al., 2020; Sharma and Mujumdar, 2017), underscoring the consistent manifestation of these patterns even on different scales. The distinct clustering of CDHs in specific regions also aligns with the heightened occurrence of these interconnected hazards in certain areas with tropical and mild temperate climates. To be specific, the hotspots of DW (i.e., East Asia and Southeast Asia) appears in the same regions as the hotspots of DFW (i.e., Southwest China and Indonesia) but with a broader coverage (refer to Fig. 5e and j). Jia and Zeyong (2017) and Albar et al. (2018) contribute to this validation as their studies corroborate the increased likelihood of compound hazards in China and Indonesia, respectively. These events also align with the disaster events recorded in Emergency Events Database (EM-DAT) from 1980 to 2021 (Supplementary Tables S1–S6). Lastly, it should be noted that a significant portion of CDHs occur in developing countries which highlights the potential impact of changes in land cover on their occurrence (Pan et al., 2023; Wei et al., 2022).

While certain studies, such as OECD (2021) and Lawrence et al. (2020), have explored the anticipated alterations of CEs in changing a climate due to altered emission conditions, the temporal trends of CEs are also directly influenced by human-related activities, such as industrial processes, deforestation, and shifts in land use. Particularly, significant increase in frequency and duration of CEs are apparent in highly urbanized regions including: southwest Russia, northwestern part of Kazakhstan, east of Uzbekistan, Mongolia, eastern China, and upper regions of South Korea (refer to Fig. 7). These findings align closely with the insights from the 2021 Asia-Pacific disaster report which identified these same regions (recognized as areas with high population density) as hotspots for exposure to cascading risks (Alisjahbana et al., 2021). Notably, high significant trends of frequency and duration of CEs can be observed in Guangdong, China (Fig. 7e, f, and 7i), which is known for its fast-growing economy and dense population. He et al. (2017) and L. Wang et al. (2022) also indicated that it ranks among the regions most susceptible to heatwave and drought mainly due to extensive human activities. Our findings, which highlight the prevalence of CEs in Asia's most populous regions, further confirm the influence of anthropogenic activities in the occurrence of these events.

In this study, we have adopted threshold-based values from established methods and experiences in the scientific literature to define the selected DHs, ensuring robust results (e.g., Abatzoglou et al., 2021; Messmer and Simmonds, 2021; Sutanto et al., 2020). While our results are quite robust with different definitions (see Text S7), it is crucial to note that modifying these threshold values may introduce potential variations in the results. For example, increasing the FWI threshold to higher percentiles might result in the detection of fewer events, potentially influencing their characteristics, as observed in previous studies (Arnell et al., 2021; Miller et al., 2023). Similarly, the pre-defined percentiles for heatwave and wind extremes may influence the occurrence of these DHs. The choice of SPI timescale is a critical consideration in drought monitoring and assessment, as it has the potential to yield diverse outcomes due to its ability to capture both short-term and long-term drought conditions (Stagge et al., 2015). Nevertheless, we diligently strived to achieve optimal outcomes through careful efforts in characterizing these DHs. Lastly, we employed the ERA5 dataset in this study; however, it is important to emphasize that acquiring results from diverse datasets is required in the future for robust inference. As a foundational step, our results provide essential groundwork for assessing the actual effects caused by the various CDHs in the study area.

6. Conclusion

Given the substantial threat posed by climate extremes leading to economic losses and ecological degradation, previous research has devoted significant attention to these extreme events. However, these

studies have primarily focused on individual hazard occurrences and may have overlooked other interconnected hazards. When multiple hazards simultaneously impact the same region, they can yield substantial consequences, as one hazardous event often worsens due to interactions with another. This underscores the importance of exploring the analysis of compound hazard occurrences. Furthermore, with the escalation in anthropogenic activities and rising temperatures in Asia, we are motivated to investigate the occurrence of compound dry hazards (CDHs) in the region. To be specific, this study explores the spatial and temporal characteristics of CDHs including drought, heatwaves, fire danger, and extreme winds across Asia from 1980 to 2021.

Guided by our four primary objectives, the key findings can be summarized as follows. First, the interannual variability in the spatial extent of CDHs across the region revealed a widespread increase in CDH occurrences. Notably, HD, HDF, HDW, DFW, and HDFW have showed concerning signs of rapid emergence as their spatial extent surges in 2021. On the other hand, when considering sub-regional analysis, the annual average frequency of CDHs exhibited a varying pattern, with DF having the highest average occurrence in all subregions. Second, hotspots of CDHs are mostly observed in low-latitude regions, predominantly across East Asia, South Asia, and Southeast Asia. Notably, a significant portion of these hotspots occur in developing countries highlighting the potential impact of changes in land cover on their occurrence. Next, temporal changes of frequency and duration of CEs reveal distinct patterns across various Asian regions. A significant increase is observed in North, Central, East, and West Asia while a notable decline is prominent in South Asia, particularly in central India. It is noted that high increases in these regions are prevalent in areas with high population density, leading to potential connections between human activities and the occurrence of CEs. These observed temporal changes substantially offer practical information for regions most susceptible to the compounded effects of DHs, such as guidance for targeted mitigation and preparedness strategies. Lastly, the dependence structure reveals that, despite all these variables (heatwave, drought, fire, extreme wind) being categorized as DHs, they still exhibit varying degrees of interdependence with each other and display a spatially diverse relationship patterns across Asian regions. This informs that aside from their individual hazard interactions, the occurrence of CDHs may also be attributed to other regional factors such as distinct local features.

Finally, we firmly believe that the findings related to CDH results and the characterization of CE events in our study hold significant value for managing natural risks in the study region. Moreover, our findings hold additional significance in the field of climatology and environment as they facilitate the critical evaluation of the accuracy of global climate models in simulating CDHs. Analyzing climate models proficient in simulating CDHs, as well as those models that accurately represent CDH statistics with the appropriate physical mechanisms, would offer planners and risk analysts a clear perspective on which climate models are most suitable for examining the evolving risks associated with compound climate extremes in the context of a changing climate.

CRediT authorship contribution statement

Davy Jean Abella: Writing – original draft, Investigation, Formal analysis, Conceptualization. **Kuk-Hyun Ahn:** Writing – review & editing, Validation, Supervision, Project administration.

Declaration of competing interest

The authors declare that they have no known competing financial interests or personal relationships that could have appeared to influence the work reported in this paper.

Data availability

Data will be made available on request.

Acknowledgment

This work was supported by the National Research Foundation of Korea (NRF) grant funded by the Korea government (MSIT) (No. RS-2023-00208210).

Appendix A. Supplementary data

Supplementary data to this article can be found online at https://doi.org/10.1016/j.wace.2024.100669.

References

Aadhar, S., Mishra, V., 2023. The 2022 mega heatwave in South Asia in the observed and projected future climate. Environ. Res. Lett. 18, 104011 https://doi.org/10.1088/1748-9326/acf778.

Abatzoglou, J.T., Juang, C.S., Williams, A.P., Kolden, C.A., Westerling, A.L., 2021. Increasing synchronous fire danger in forests of the western United States. Geophys. Res. Lett. 48 https://doi.org/10.1029/2020GL091377.

Abram, N.J., Henley, B.J., Sen Gupta, A., Lippmann, T.J.R., Clarke, H., Dowdy, A.J., Sharples, J.J., Nolan, R.H., Zhang, T., Wooster, M.J., Wurtzel, J.B., Meissner, K.J., Pitman, A.J., Ukkola, A.M., Murphy, B.P., Tapper, N.J., Boer, M.M., 2021. Connections of climate change and variability to large and extreme forest fires in southeast Australia. Commun Earth Environ 2, 8. https://doi.org/10.1038/s43247-020-00065-8.

Afroz, M., Chen, G., Anandhi, A., 2023. Drought-and heatwave-associated compound extremes: a review of hotspots, variables, parameters, drivers, impacts, and analysis frameworks. Front. Earth Sci. 10, 914437.

AghaKouchak, A., Chiang, F., Huning, L.S., Love, C.A., Mallakpour, I., Mazdiyasni, O., Moftakhari, H., Papalexiou, S.M., Ragno, E., Sadegh, M., 2020. Climate extremes and compound hazards in a warming world. Annu. Rev. Earth Planet Sci. 48, 519–548. https://doi.org/10.1146/annurev-earth-071719-055228.

AghaKouchak, A., Huning, L.S., Chiang, F., Sadegh, M., Vahedifard, F., Mazdiyasni, O., Moftakhari, H., Mallakpour, I., 2018. How do natural hazards cascade to cause disasters? Nature 561, 458–460. https://doi.org/10.1038/d41586-018-06783-6.

Ahn, K.-H., 2022. Interannual variability of heat waves over the Korean Peninsula based on integrated approach. Sci. Total Environ. 826, 154153 https://doi.org/10.1016/j.scitotenv.2022.154153.

Albar, I., Jaya, I.N.S., Saharjo, B.H., Kuncahyo, B., Vadrevu, K.P., 2018. Spatio-temporal analysis of land and forest fires in Indonesia using MODIS active fire dataset. Land-atmospheric research applications in South and Southeast Asia 105–127.

Alisjahbana, A., Zahedi, K., Bonapace, T., 2021. Resilience in a Riskier World: Asia-Pacific Disaster Report 2021.

Alizadeh-Choobari, O., Ghafarian, P., Owlad, E., 2016. Temporal variations in the frequency and concentration of dust events over Iran based on surface observations: climatology of dust events over Iran. Int. J. Climatol. 36, 2050–2062. https://doi.org/10.1002/joc.4479.

Arnell, N., Freeman, A., Gazzard, R., 2021. The effect of climate change on indicators of fire danger in the UK. Environ. Res. Lett. 16, 044027.

Baldwin, J.W., Dessy, J.B., Vecchi, G.A., Oppenheimer, M., 2019. Temporally compound heat wave events and global warming: an emerging hazard. Earth's Future 7, 411–427. https://doi.org/10.1029/2018EF000989.

Bell, B., Hersbach, H., Simmons, A., Berrisford, P., Dahlgren, P., Horányi, A., Muñoz-Sabater, J., Nicolas, J., Radu, R., Schepers, D., Soci, C., Villaume, S., Bidlot, J., Haimberger, L., Woollen, J., Buontempo, C., Thépaut, J., 2021. The ERA5 global reanalysis: preliminary extension to 1950. Q. J. R. Meteorol. Soc. 147, 4186–4227. https://doi.org/10.1002/qj.4174.

Buckley, B.M., Fletcher, R., Wang, S.-Y.S., Zottoli, B., Pottier, C., 2014. Monsoon extremes and society over the past millennium on mainland Southeast Asia. Quat. Sci. Rev. 95, 1–19. https://doi.org/10.1016/j.quascirev.2014.04.022.

Das, J., Gayen, A., Saha, P., Bhattacharya, S.K., 2020. Meteorological drought analysis using standardized precipitation index over luni river basin in Rajasthan, India. SN Appl. Sci. 2, 1530. https://doi.org/10.1007/s42452-020-03321-w.

Depietri, Y., Dahal, K., McPhearson, T., 2018. Multi-hazard risks in New York city. Nat. Hazards Earth Syst. Sci. 18, 3363–3381. https://doi.org/10.5194/nhess-18-3363-2018.

Dilley, M., 2005. Natural Disaster Hotspots: a Global Risk Analysis. World Bank Publications.

Dupire, S., Curt, T., Bigot, S., 2017. Spatio-temporal trends in fire weather in the French Alps. Sci. Total Environ. 595, 801–817. https://doi.org/10.1016/j.scitotenv.2017.04.027.

Evers, C., Holz, A., Busby, S., Nielsen-Pincus, M., 2022. Extreme winds alter influence of fuels and topography on megafire burn severity in seasonal temperate rainforests under record fuel aridity. Fire 5, 41. https://doi.org/10.3390/fire5020041.

Gill, J.C., Malamud, B.D., 2014. Reviewing and visualizing the interactions of natural hazards: interactions of Natural Hazards. Rev. Geophys. 52, 680–722. https://doi.org/10.1002/2013RG000445.

Good, P., Moriondo, M., Giannakopoulos, C., Bindi, M., 2008. The meteorological conditions associated with extreme fire risk in Italy and Greece: relevance to climate model studies. Int. J. Wildland Fire 17, 155–165.

Goss, M., Swain, D.L., Abatzoglou, J.T., Sarhadi, A., Kolden, C.A., Williams, A.P., Diffenbaugh, N.S., 2020. Climate change is increasing the likelihood of extreme

autumn wildfire conditions across California. Environ. Res. Lett. 15, 094016 https://doi.org/10.1088/1748-9326/ab83a7.
Gu, D., 2019. Exposure and vulnerability to natural disasters for world's cities. Population Division. Department of Economics and Social Affairs, United Nations. Technical Paper No. 4.
He, Y., Lin, K., Tang, G., Chen, X., Guo, S., Gui, F., 2017. Quantifying the changing properties of climate extremes in Guangdong Province using individual and integrated climate indices: quantifying the changing properties of climate extremes. Int. J. Climatol. 37, 781–792. https://doi.org/10.1002/joc.4739.
Henson, B., 2020. Heat, drought, and fire striking early in Asia. Category 6 news site at Weather Underground. https://www.wunderground.com/cat6/heat-drought-and-fire-striking-early-in-asia.
Herrera García, S., Bedía Jiménez, J., Gutiérrez Llorente, J.M., Moreno Rodríguez, J.M., 2013. On the Projection of Future Fire Danger Conditions with Various Instantaneous/mean-Daily Data Sources.
Hersbach, H., Bell, B., Berrisford, P., Hirahara, S., Horányi, A., Muñoz-Sabater, J., Nicolas, J., Peubey, C., Radu, R., Schepers, D., Simmons, A., Soci, C., Abdalla, S., Abellan, X., Balsamo, G., Bechtold, P., Biavati, G., Bidlot, J., Bonavita, M., Chiara, G., Dahlgren, P., Dee, D., Diamantakis, M., Dragani, R., Flemming, J., Forbes, R., Fuentes, M., Geer, A., Haimberger, L., Healy, S., Hogan, R.J., Hólm, E., Janisková, M., Keeley, S., Laloyaux, P., Lopez, P., Lupu, C., Radnoti, G., Rosnay, P., Rozum, I., Vamborg, F., Villaume, S., Thépaut, J., 2020. The ERA5 global reanalysis. Q. J. R. Meteorol. Soc. 146, 1999–2049. https://doi.org/10.1002/qj.3803.
IPCC, 2022. In: Pörtner, H.-O., Roberts, D.C., Tignor, M., Poloczanska, E.S., Mintenbeck, K., Alegría, A., Craig, M., Langsdorf, S., Löschke, S., Möller, V., Okem, A., Rama, B. (Eds.), Climate Change 2022: Impacts, Adaptation and Vulnerability. Contribution of Working Group II to the Sixth Assessment Report of the Intergovernmental Panel on Climate Change. Cambridge University Press. Cambridge University Press, Cambridge, UK and New York, NY, USA, p. 3056. https://doi.org/10.1017/9781009325844.
Jia, J., Zeyong, H., 2017. Spatial and temporal features and trend of different level heat waves over China. Adv. Earth Sci. 32, 546.
Jiao, D., Xu, N., Yang, F., Xu, K., 2021. Evaluation of spatial-temporal variation performance of ERA5 precipitation data in China. Sci. Rep. 11, 17956 https://doi.org/10.1038/s41598-021-97432-y.
Kendall, M.G., 1948. Rank Correlation Methods.
Kong, Q., Guerreiro, S.B., Blenkinsop, S., Li, X.-F., Fowler, H.J., 2020. Increases in summertime concurrent drought and heatwave in Eastern China. Weather Clim. Extrem. 28, 100242 https://doi.org/10.1016/j.wace.2019.100242.
Lan, H., Guo, D., Hua, W., Pepin, N., Sun, J., 2023. Evaluation of reanalysis air temperature and precipitation in high-latitude Asia using ground-based observations. Intl Journal of Climatology 43, 1621–1638. https://doi.org/10.1002/joc.7937.
Lawrence, J., Blackett, P., Cradock-Henry, N.A., 2020. Cascading climate change impacts and implications. Climate Risk Management 29, 100234. https://doi.org/10.1016/j.crm.2020.100234.
Leonard, M., Westra, S., Phatak, A., Lambert, M., van den Hurk, B., McInnes, K., Risbey, J., Schuster, S., Jakob, D., Stafford-Smith, M., 2014. A compound event framework for understanding extreme impacts. WIREs Climate Change 5, 113–128. https://doi.org/10.1002/wcc.252.
Libonati, R., Geirinhas, J.L., Silva, P.S., Russo, A., Rodrigues, J.A., Belém, L.B.C., Nogueira, J., Roque, F.O., DaCamara, C.C., Nunes, A.M.B., Marengo, J.A., Trigo, R. M., 2022. Assessing the role of compound drought and heatwave events on unprecedented 2020 wildfires in the Pantanal. Environ. Res. Lett. 17, 015005 https://doi.org/10.1088/1748-9326/ac462e.
Littell, J.S., Peterson, D.L., Riley, K.L., Liu, Y., Luce, C.H., 2016. A review of the relationships between drought and forest fire in the United States. Global Change Biol. 22 (7), 2353–2369. https://doi.org/10.1111/gcb.13275.
Liu, M., Yin, Y., Wang, X., Ma, X., Chen, Y., Chen, W., 2022. More frequent, long-lasting, extreme and postponed compound drought and hot events in eastern China. J. Hydrol. 614, 128499 https://doi.org/10.1016/j.jhydrol.2022.128499.
Mann, H.B., 1945. Nonparametric tests against trend. Econometrica: J. Econom. Soc. 245–259.
Martius, O., Pfahl, S., Chevalier, C., 2016. A global quantification of compound precipitation and wind extremes: compound precipitation and wind extremes. Geophys. Res. Lett. 43, 7709–7717. https://doi.org/10.1002/2016GL070017.
Mass, C.F., Ovens, D., 2019. The northern California wildfires of 8–9 october 2017: the role of a major downslope wind event. Bull. Am. Meteorol. Soc. 100, 235–256. https://doi.org/10.1175/BAMS-D-18-0037.1.
Mazdiyasni, O., AghaKouchak, A., 2015. Substantial increase in concurrent droughts and heatwaves in the United States. Proc. Natl. Acad. Sci. U.S.A. 112, 11484–11489. https://doi.org/10.1073/pnas.1422945112.
McKee, T., Doesken, N., Kleist, J., 1993. The relationship of drought frequency and duration to time scales. Eighth Conf on Applied Climatology Anaheim CA. Amer Meteor Soc 179–184.
Meng, Y., Hao, Z., Zhang, Y., Feng, S., 2023. The 2022-like compound dry and hot extreme in the Northern Hemisphere: extremeness, attribution, and projection. Atmos. Res. 295, 107009 https://doi.org/10.1016/j.atmosres.2023.107009.
Messmer, M., Simmonds, I., 2021. Global analysis of cyclone-induced compound precipitation and wind extreme events. Weather Clim. Extrem. 32, 100324 https://doi.org/10.1016/j.wace.2021.100324.
Miller, J., Böhnisch, A., Ludwig, R., Brunner, M.I., 2023. Climate change impacts on regional fire weather in heterogeneous landscapes of Central Europe (preprint). Atmospheric, Meteorological and Climatological Hazards. https://doi.org/10.5194/nhess-2023-51.
Miyan, M.A., 2015. Droughts in asian least developed countries: vulnerability and sustainability. Weather Clim. Extrem. 7, 8–23. https://doi.org/10.1016/j.wace.2014.06.003.
Mukherjee, S., Mishra, A.K., 2021. Increase in compound drought and heatwaves in a warming world. Geophys. Res. Lett. 48 https://doi.org/10.1029/2020GL090617.
NOAA National Centers for Environmental Information, Monthly Global Climate Report for Annual 2020. published online January 2021. https://www.ncei.noaa.gov/access/monitoring/monthly-report/global/202013.
Nosrati, K., Zareiee, A.R., 2011. Assessment of meteorological drought using SPI in west azarbaijan province, Iran. J. Appl. Sci. Environ. Manag. 15, 563–569.
OECD, 2021. Climate change impacts and their cascading effects: implications for losses and damages. In: Managing Climate Risks, Facing up to Losses and Damages. OECD. https://doi.org/10.1787/f50ec22e-en.
Osman, M., Zaitchik, B.F., Winstead, N.S., 2022. Cascading drought-heat dynamics during the 2021 southwest United States heatwave. Geophys. Res. Lett. 49 https://doi.org/10.1029/2022GL099265.
Pan, R., Li, W., Wang, Q., Ailiyaer, A., 2023. Detectable anthropogenic intensification of the summer compound hot and dry events over global land areas. Earth's Future 11, e2022EF003254. https://doi.org/10.1029/2022EF003254.
Paprotny, D., Vousdoukas, M.I., Morales-Nápoles, O., Jonkman, S.N., Feyen, L., 2018. Compound flood potential in Europe (preprint). Hydrometeorology/Mathematical applications. https://doi.org/10.5194/hess-2018-132.
Patel, N., Chopra, P., Dadhwal, V., 2007. Analyzing spatial patterns of meteorological drought using standardized precipitation index. Meteorol. Appl.: A journal of forecasting, practical applications, training techniques and modelling 14, 329–336.
Perkins-Kirkpatrick, S.E., Lewis, S.C., 2020. Increasing trends in regional heatwaves. Nat. Commun. 11, 3357. https://doi.org/10.1038/s41467-020-16970-7.
Pescaroli, G., Alexander, D., 2018. Understanding compound, interconnected, interacting, and cascading risks: a holistic framework: a holistic framework for understanding complex risks. Risk Anal. 38, 2245–2257. https://doi.org/10.1111/risa.13128.
Population of Asia (2023) - Worldometer, 2023. https://www.worldometers.info/world-population/asia-population/.
Pu, B., Jin, Q., Ginoux, P., Yu, Y., 2022. Compound heat wave, drought, and dust events in California. J. Clim. 35, 8133–8152. https://doi.org/10.1175/JCLI-D-21-0889.1.
Ridder, N.N., Pitman, A.J., Westra, S., Ukkola, A., Do, H.X., Bador, M., Hirsch, A.L., Evans, J.P., Di Luca, A., Zscheischler, J., 2020. Global hotspots for the occurrence of compound events. Nat. Commun. 11, 5956. https://doi.org/10.1038/s41467-020-19639-3.
Ridder, N.N., Ukkola, A.M., Pitman, A.J., Perkins-Kirkpatrick, S.E., 2022. Increased occurrence of high impact compound events under climate change. npj Clim Atmos Sci 5, 3. https://doi.org/10.1038/s41612-021-00224-4.
Russo, S., Dosio, A., Sterl, A., Barbosa, P., Vogt, J., 2013. Projection of occurrence of extreme dry-wet years and seasons in Europe with stationary and nonstationary Standardized Precipitation Indices: wetness and drought in Europe. J. Geophys. Res. Atmos. 118, 7628–7639. https://doi.org/10.1002/jgrd.50571.
Semenova, I., Sumak, K., 2022. Dynamics of fire weather conditions in the mixed forest areas of Belarus and Ukraine under recent climate change. Geofizika 39, 71–83. https://doi.org/10.15233/gfz.2022.39.10.
Sen, P.K., 1968. Estimates of the regression coefficient based on Kendall's tau. J. Am. Stat. Assoc. 63, 1379–1389.
Shafiei Shiva, J., Chandler, D.G., Kunkel, K.E., 2022. Mapping heat wave hazard in urban areas: a novel multi-criteria decision making approach. Atmosphere 13, 1037. https://doi.org/10.3390/atmos13071037.
Sharma, A., Andhikaputra, G., Wang, Y.-C., 2022. Heatwaves in South Asia: characterization, consequences on human health, and adaptation strategies. Atmosphere 13, 734. https://doi.org/10.3390/atmos13050734.
Sharma, S., Mujumdar, P., 2017. Increasing frequency and spatial extent of concurrent meteorological droughts and heatwaves in India. Sci. Rep. 7, 15582 https://doi.org/10.1038/s41598-017-15896-3.
Silva, P.S., Geirinhas, J.L., Lapere, R., Laura, W., Cassain, D., Alegría, A., Campbell, J., 2022. Heatwaves and fire in Pantanal: historical and future perspectives from CORDEX-CORE. J. Environ. Manag. 323, 116193 https://doi.org/10.1016/j.jenvman.2022.116193.
Spinoni, J., Naumann, G., Carrao, H., Barbosa, P., Vogt, J., 2014. World drought frequency, duration, and severity for 1951-2010: world drought climatologies for 1951-2010. Int. J. Climatol. 34, 2792–2804. https://doi.org/10.1002/joc.3875.
Srock, A., Charney, J., Potter, B., Goodrick, S., 2018. The hot-dry-windy index: a new fire weather index. Atmosphere 9, 279. https://doi.org/10.3390/atmos9070279.
Stagge, J.H., Tallaksen, L.M., Gudmundsson, L., Van Loon, A.F., Stahl, K., 2015. Candidate distributions for climatological drought indices (SPI and SPEI). Int. J. Climatol. 35, 4027–4040.
Stefanon, M., D'Andrea, F., Drobinski, P., 2012. Heatwave classification over Europe and the mediterranean region. Environ. Res. Lett. 7, 014023 https://doi.org/10.1088/1748-9326/7/1/014023.
Sutanto, S.J., Vitolo, C., Di Napoli, C., D'Andrea, M., Van Lanen, H.A.J., 2020. Heatwaves, droughts, and fires: exploring compound and cascading dry hazards at the pan-European scale. Environ. Int. 134, 105276 https://doi.org/10.1016/j.envint.2019.105276.
Tavakol, A., Rahmani, V., Harrington, J., 2020. Temporal and spatial variations in the frequency of compound hot, dry, and windy events in the central United States. Sci. Rep. 10, 15691 https://doi.org/10.1038/s41598-020-72624-0.
Van Wagner, C., 1987. Development and Structure of the Canadian Forest Fire Weather Index System.
Van Wagner, C.E., 1974. Structure of the Canadian Forest Fire Weather Index. Environment Canada, Forestry Service Alberta, Canada.

Varela, V., Sfetsos, A., Vlachogiannis, D., Gounaris, N., 2018. Fire Weather Index (FWI) classification for fire danger assessment applied in Greece. Tethys 15, 31–40.
Wang, C., Li, Z., Chen, Y., Li, Y., Liu, X., Hou, Y., Wang, X., Kulaixi, Z., Sun, F., 2022. Increased compound droughts and heatwaves in a double pack in central Asia. Rem. Sens. 14, 2959. https://doi.org/10.3390/rs14132959.
Wang, L., Hu, F., Zhang, C., Miao, Y., Chen, H., Zhong, K., Luo, M., 2022. Response of vegetation to different climate extremes on a monthly scale in Guangdong, China. Rem. Sens. 14, 5369. https://doi.org/10.3390/rs14215369.
Wang, N., Xue, X., Zhang, L., Chu, Y., Jiang, M., Wang, Y., Yang, Y., Guo, X., Zhao, Y., Zhao, E., 2022. Spatial zoning of dry-hot wind disasters in shandong province. Sustainability 14, 3904. https://doi.org/10.3390/su14073904.
Wahl, T., Jain, S., Bender, J., Meyers, S.D., Luther, M.E., 2015. Increasing risk of compound flooding from storm surge and rainfall for major US cities. Nat. Clim. Chang. 5 (12), 1093–1097. https://doi.org/10.1038/nclimate2736.
Wang, T., Dai, J., Lam, K.S., Nan Poon, C., Brasseur, G.P., 2019. Twenty-five years of lower tropospheric ozone observations in tropical East Asia: the influence of emissions and weather patterns. Geophys. Res. Lett. 46, 11463–11470. https://doi.org/10.1029/2019GL084459.
Ward, P.J., Blauhut, V., Bloemendaal, N., Daniell, J.E., De Ruiter, M.C., Duncan, M.J., Emberson, R., Jenkins, S.F., Kirschbaum, D., Kunz, M., Mohr, S., Muis, S., Riddell, G. A., Schäfer, A., Stanley, T., Veldkamp, T.I.E., Winsemius, H.C., 2020. Review article: natural hazard risk assessments at the global scale. Nat. Hazards Earth Syst. Sci. 20, 1069–1096. https://doi.org/10.5194/nhess-20-1069-2020.
Wei, X., Huang, S., Huang, Q., Liu, D., Leng, G., Yang, H., Duan, W., Li, J., Bai, Q., Peng, J., 2022. Analysis of vegetation vulnerability dynamics and driving forces to multiple drought stresses in a changing environment. Rem. Sens. 14, 4231. https://doi.org/10.3390/rs14174231.
WMO statement on the state of the global climate in 2021 = State of the Global Climate 2021, 2022. World Meteorological Organization (WMO).
Xu, X., He, S., Gao, Y., Furevik, T., Wang, H., Li, F., Ogawa, F., 2019. Strengthened linkage between midlatitudes and Arctic in boreal winter. Clim. Dynam. 53, 3971–3983. https://doi.org/10.1007/s00382-019-04764-7.
Yang, Y., Maraun, D., Ossó, A., Tang, J., 2023. Increased spatial extent and likelihood of compound long-duration dry and hot events in China, 1961–2014. Nat. Hazards Earth Syst. Sci. 23, 693–709. https://doi.org/10.5194/nhess-23-693-2023.
Yu, H., Lu, N., Fu, B., Zhang, L., Wang, M., Tian, H., 2022. Hotspots, co-occurrence, and shifts of compound and cascading extreme climate events in Eurasian drylands. Environ. Int. 169, 107509 https://doi.org/10.1016/j.envint.2022.107509.
Zhang, R., Bento, V.A., Qi, J., Xu, F., Wu, J., Qiu, J., Li, J., Shui, W., Wang, Q., 2023. The first high spatial resolution multi-scale daily SPI and SPEI raster dataset for drought monitoring and evaluating over China from 1979 to 2018. Big Earth Data 1–26. https://doi.org/10.1080/20964471.2022.2148331.
Zittis, G., Almazroui, M., Alpert, P., Ciais, P., Cramer, W., Dahdal, Y., Fnais, M., Francis, D., Hadjinicolaou, P., Howari, F., Jrrar, A., Kaskaoutis, D.G., Kulmala, M., Lazoglou, G., Mihalopoulos, N., Lin, X., Rudich, Y., Sciare, J., Stenchikov, G., Xoplaki, E., Lelieveld, J., 2022. Climate change and weather extremes in the eastern mediterranean and Middle East. Rev. Geophys. 60 https://doi.org/10.1029/2021RG000762.
Zscheischler, J., Martius, O., Westra, S., Bevacqua, E., Raymond, C., Horton, R.M., van den Hurk, B., AghaKouchak, A., Jézéquel, A., Mahecha, M.D., Maraun, D., Ramos, A. M., Ridder, N.N., Thiery, W., Vignotto, E., 2020. A typology of compound weather and climate events. Nat. Rev. Earth Environ. 1, 333–347. https://doi.org/10.1038/s43017-020-0060-z.
Zscheischler, J., Seneviratne, S.I., 2017. Dependence of drivers affects risks associated with compound events. Sci. Adv. 3, e1700263 https://doi.org/10.1126/sciadv.1700263.